

This is the **accepted version** of the article:

Llacer-Wintle, Joaquin; Rivas-Dapena, Antón; Chen, Xiang-Zhong; [et al.].
«Biodegradable small-scale swimmers for biomedical applications». Advanced
Materials, (September 2021). DOI 10.1002/adma.202102049

This version is available at <https://ddd.uab.cat/record/249626>

under the terms of the  **IN**
COPYRIGHT license

Biodegradable Small-Scale Swimmers for Biomedical Applications

Joaquin Llacer-Wintle, Antón Rivas-Dapena, Xiang-Zhong Chen, Eva Pellicer, Bradley J. Nelson, Josep Puigmartí-Luis, Salvador Pané,

Abstract

Most forms of biomatter are ephemeral, which means they transform or deteriorate after a certain time. From this perspective, implantable healthcare devices designed for temporary treatments should exhibit the ability to degrade and either blend in with healthy tissues, or be cleared from the body with minimal disruption after accomplishing their designated tasks. This topic is currently being investigated in the field of biomedical micro- and nanoswimmers. These tiny devices have the ability to move through fluids by converting physical or chemical energy into motion. Several architectures of these devices have been designed to mimic the motion strategies of nature's motile microorganisms and cells. Due to their motion abilities, these devices have been proposed as minimally invasive tools for precision healthcare applications. Hence, a natural progression in this field is to produce motile structures that can adopt, or even surpass, similar transient features as biological systems. The fate of small-scale swimmers after accomplishing their therapeutic mission is critical for the successful translation of small-scale swimmers' technologies into clinical applications. In this review, recent research efforts are summarized on the topic of biodegradable micro- and nanoswimmers for biomedical applications, with a focus on targeted therapeutic delivery.

1 Introduction

Small-scale swimmers are micro- and nanodevices constructed with active materials that respond to physical (e.g., magnetic, photonic, electric, acoustic) or chemical stimuli, which are ultimately transduced into mechanical motion.^[1-8] The locomotion and cargo capabilities of these tiny untethered machines in biofluids offer great opportunities for medical applications. Conventional micro- and nanoparticles have demonstrated outstanding potential for biomedical applications over the last decades.^[9, 10] However, the translation of micro- and nanoparticle-based therapies is usually limited due to their low accumulation into the target cells/tissues, leading to low treatment efficiency and undesired side effects.^[11] Micro- and nanoswimmers represent a promising alternative to overcome this limitation. Thanks to their characteristic non-reciprocal movement, small-scale swimmers are able to effectively move in low Reynolds number regimes and overcome the viscous forces within biological fluids such as blood.^[1, 12] This enables small-scale swimmers to actively reach the therapeutic target and dramatically increase the efficiency of potential treatments.^[2] The incorporation of therapeutic and diagnostic components in micro- and nanoswimmers is opening the door to applications in targeted drug/cell delivery, detoxification, microsurgery, localized diagnosis and tissue regeneration.^[2, 13-15] The successful translation of small-scale swimmers from the test tube to the bedside will lead to the development of minimally invasive operations with reduced risks and costs, and minimal patient discomfort. The field of small-scale swimmers has made astounding progress over the last two decades,^[16-19] with the main focus being on the locomotion and

functionalization of these machines. For the fundamentals on the locomotion at small-scales, please refer to previous reviews.^[4, 7, 20-22] Recently, several motile small-scale devices have been successfully implanted into the bodies of living animals, and some investigations have demonstrated their therapeutic value.^[23-27] However, several aspects still have to be addressed for the application of micro- and nanoswimmers into clinical practice, including in vivo imaging and monitoring, biocompatibility, and the optimal therapeutic cargo/number of swimmers. The requirements of a swimmer are strongly dependent upon the end application. For instance, swimmers designed for biopsies should be long-term chemically stable and easily retrievable.^[28] In contrast, post-application device retrieval seems unnecessary for targeted therapeutic delivery. The safest strategy for micro- and nanoswimmers with predefined delivery tasks involves construction with building blocks, the degradation products of which are nontoxic and can be eventually resorbed. In fact, the same strategy is also applied in the field of non-invasive and minimally invasive sensors for personalized medicine and sport and wellness. Some challenges, such as stability of the active parts, degradation lifetime, on-demand triggered degradation and long-term bio-compatibility in vivo are shared across the fields of small-scale swimmers and minimally invasive implantable sensors.^[29, 30] Note that different terms (absorption, bioassimilation, biodegradation, bioresorption, etc.) are found in literature to describe the degradation and removal of materials used for biomedical purposes.^[31, 32] Depending on the context, these terms may have subtle differences, or one may be preferred over the others. Therefore, to avoid possible misconceptions and make the reading simpler, we will use the term “biodegradable” to refer to a material that experiences physical and/or chemical deleterious changes of its integrity in physiological conditions, either in vivo or in vitro. These changes can occur in different ways, i.e., degradation mechanisms: enzymatic degradation, hydrolytic degradation, photodegradation or thermal degradation, among others. On the other hand, we will use the term “bioresorbable” to refer to a substance that fully vanishes from the organism by the process of metabolism, secretion or excretion. While it has gradually been recognized that developing transient swimmers for targeted therapeutic delivery is of great importance to clinical applications, research in this topic is still in its infancy.

This review summarises the research efforts on the topic of biodegradable micro- and nanoswimmers for biomedical applications, with a main focus on targeted therapeutic delivery. These swimmers include those powered by external physical energy sources like magnetic fields (Section 2), ultrasound or light (Section 3); by chemical fuels (Section 4); or by living organisms (Section 5). Note that depending on the level of motion control, the micro- and nanoswimmers will be defined as small-scale robots or motors. While the motion of small-scale robots can be precisely controlled through external stimuli (e.g., with magnetic fields and/or acoustic fields, among others), enabling their acceleration in any desired direction of the space or their complete cease of motion, small-scale swimmers that move erratically are designated as motors. For a better understanding of these concepts, we refer the readers to the referenced review.^[33] Small-scale swimmers often integrate several components with different functionalities such as motion, sensing, imaging or

treatment, among others. Considering the complexity of some swimmer designs, we will summarise not only fully biodegradable devices, but also those that contain biodegradable building blocks. Our aim is to review as many examples as possible to give a general overview of swimmers' biodegradability, and provide a good source of reference and inspiration for future endeavors in this field.

2 Magnetically Driven Biodegradable Small-Scale Swimmers

Magnetically driven small-scale swimmers, also known as magnetic micro- and nanorobots, are miniaturized devices that can be actuated using magnetic field gradients or time-varying magnetic fields. Magnetic gradients are used to pull or drag magnetically responsive objects as a result of a generated force (Equation (1)). Magnetic objects can also oscillate or rotate when subject to time-varying magnetic fields due to an induced torque (Equation (2)). Depending on the geometric characteristics and the magnetic history of the object,^[34] oscillating magnetic fields can be used to generate different locomotion patterns, ranging from rolling, tumbling and precession, to corkscrew or travelling-wave propulsion. For the fundamentals of magnetic manipulation, we refer the reader to a recent review by Abbott and coworkers^[1]

$$\vec{F} \approx (\vec{m} \cdot \nabla) \vec{B}_e \quad (1)$$

$$\vec{\tau} \approx \vec{m} \times \vec{B}_e(t) \quad (2)$$

where \vec{F} and $\vec{\tau}$ are the generated magnetic force and magnetic torque, respectively, \vec{m} is the magnetic moment of the swimmer, and \vec{B}_e is the magnetic field flux density.

Magnetic manipulation is well suited to biomedical applications, as magnetic fields can permeate through organisms without causing any harm to tissues in a wide range of frequencies and magnitudes.^[35] Therefore, magnetic actuation is one of the most investigated approaches for driving micro- and nanoswimmers for clinical applications. In general, time-varying magnetic fields are preferred over magnetic field gradients for the manipulation of magnetic objects, as the former can be projected at longer distances than the latter.^[1] The vast majority of magnetic micro- and nanorobots are made of ferromagnetic, ferrimagnetic or superparamagnetic building blocks, mainly in the form of metals, alloys or ceramics. Note that in this review, diamagnetic and paramagnetic devices will not be discussed, and we will only focus on objects with ferro/ferrimagnetic and superparamagnetic behavior. These materials contain at least one of the three ferromagnetic elements in the periodic table: iron, cobalt and nickel. Literature is rich in examples of micro- and nanorobots made of these metals or their alloys, but their suitability as transient devices is limited by their toxicity or that of the ions released. Fe^{2+} , Co^{2+} and Ni^{2+} are well known to participate in the formation of reactive oxygen species (ROS) involved in cell damage, but the inferior number of mechanisms to regulate the homeostasis of Co^{2+} and Ni^{2+} and their added carcinogenic potential make iron-based micro- and nanorobots a better choice for biomedical purposes.^[36-38]

Iron and iron oxides are biocompatible in reasonable doses,^[39, 40] and are therefore suitable as magnetic components for micro- and nanorobots. Alcantara et al. fabricated fully Fe microrobots by 3D template-assisted electrodeposition. These magnetic microrobots are interesting because they exhibit large magnetic moments, which is a desired feature for their magnetic maneuverability. The biocompatibility of the Fe microrobots was tested by culturing them with HCT116 human colorectal cancer cells, and no sign of cytotoxicity was found after 4 days of incubation. The microrobots were completely degraded after 20 min of incubation in a simulated gastric acid medium (**Figure 1A**).^[41]

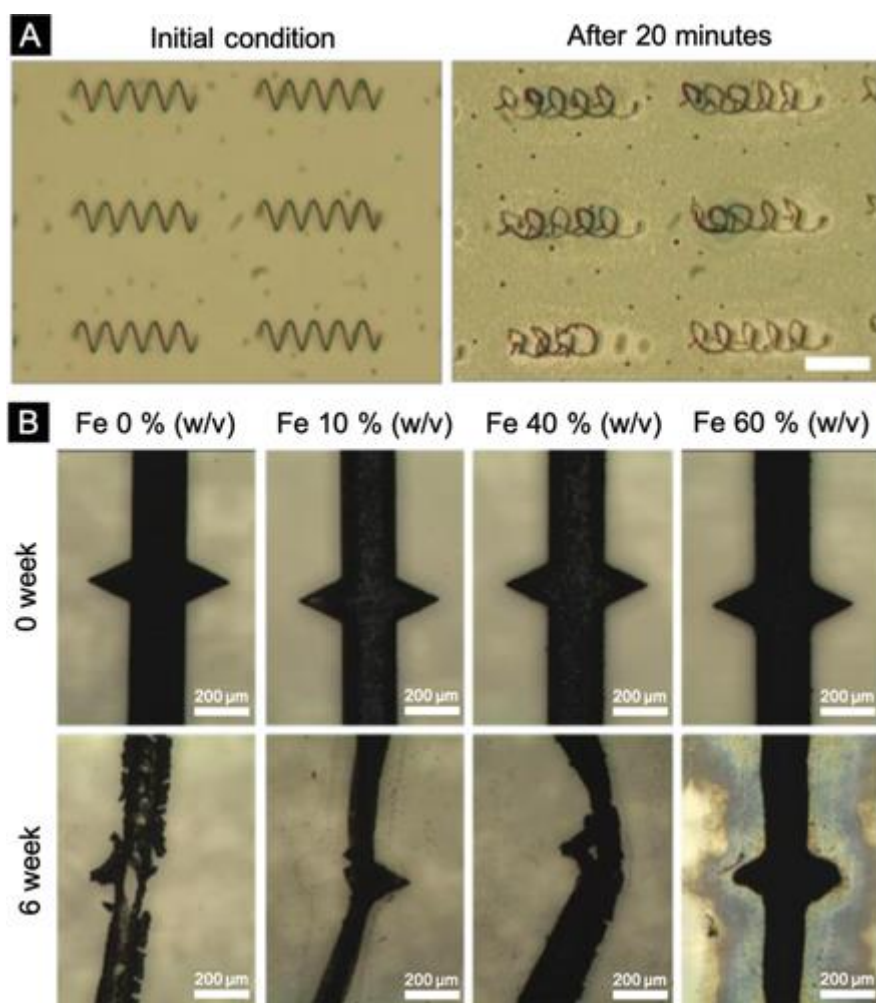


Figure 1

A) Degradation of metallic Fe microrobots in simulated gastric liquid before and after 20 min. Scale bar: 50 μm . Adapted with permission.^[41] Copyright 2019, Wiley-VCH. B) Degradation of PLGA/Fe/5-fluorouracil microrobots with Fe concentrations of 0, 10, 40, and 60% (w/v) in PBS at 37 °C over a period of 6 weeks. Scale bar: 200 μm . Adapted with permission.^[48] Copyright 2018, Elsevier B.V.

While iron and some of its alloys and oxides exhibit biocompatible characteristics, their biodegradability and/or bioresorbability may be severely hindered by the size of the iron component.^[42] To this end, NPs with sizes ranging from 10 to 200 nm can be used as magnetic building blocks for magnetic small-scale robots. However, assembling NPs to create entire 3D magnetic bodies such as helices or other architectures is challenging, and only very simple architectures can be created. Recently, researchers have proposed the use of swarms of magnetic

NPs. However, the downside of swarms is that the particulates are loosely attached and fractions of particles can easily be detached during navigation in high-flow rate bodily fluids.^[43] To this end, composites of NPs made of polymer matrices can be used to create fully biodegradable micro- and nanorobotic platforms. The use of polymer matrices is advantageous because composites can be processed in several shapes and can prevent unintended degradation before the micro- and nanorobots reach a predefined destination. Additionally, polymer matrices can serve as reservoirs to encapsulate other functional components or therapeutic payloads. Several examples can be found in literature showing the combination of iron or iron oxides and organic networks. The latter allow for on-site sustained release of drugs and, importantly, endow the composite with chemical tunability without severely compromising the magnetic moment.^[44] Drugs, contrast agents and stimuli-responsive groups can be easily attached to, or embedded within, organic networks, endowing these robots with simultaneous therapeutic and diagnostic functionalities. This feature, together with the ability to be degraded once in the target region, makes these small-scale robots promising candidates for drug delivery applications.

In this context, magnetic small-scale robots with aliphatic polyesters, i.e., poly(D,L-lactic-co-glycolic acid) (PLGA), poly(L-lactic acid) (PLLA), poly(D,L-lactic acid) (PDLLA), poly(caprolactone) (PCL), etc., have recently been a subject of research since they are biocompatible and hydrolytically degradable. In their pioneering study, Asmatulu et al. proved the targeting capabilities of magnetite-loaded PLLA and PDLLA magnetic microrobots in an artery model under a magnetic gradient.^[45] Pouponneau et al. took this concept a step further and fabricated PLGA microrobots loaded with doxorubicin (DOX) and Fe-Co NPs that could be steered with a magnetic gradient into the right or left lobes of rabbit livers. The authors claimed their microrobots could serve as an efficient chemoembolization treatment for liver tumors.^[46, 47] Kim et al. produced PLGA magnetic microrobots via a template-assisted approach. In brief, poly(vinyl alcohol) (PVA) micromachined templates were dip-coated with a mixture of PLGA, Fe microparticles (MPs) and anti-cancer drug 5-fluorouracil. The PVA templates were dissolved in an aqueous solution leaving behind the biodegradable PLGA-coated magnetic microrobots, which were actuated using magnetic field gradients. It took around 6 weeks to degrade the microrobots in PBS solution (pH 7.4, 37 °C). Interestingly, microrobots with higher concentrations of magnetic MPs degraded slower, suggesting that the particles hindered the hydrolysis of the PLGA (Figure 1B). The biocompatibility of the drug-free microrobots and the effective drug release and cytotoxicity towards HCT116 cells of drug-loaded microrobots were proven through viability assays.^[48]

Hydrogels, which are networks of cross-linked hydrophilic polymers, have also been used as scaffolds for magnetic microrobots. A biodegradable hydrogel is produced by implementing bio-cleavable bonds into its structure, either in the polymer backbone or as part of the cross-linking agent.^[49] In order to fabricate microrobots with specific geometries to meet the actuation requirement, photo-reactive groups (e.g., acrylate, methacrylate) can be introduced into hydrogel precursors, which can be photo-crosslinked by two-photon polymerization (TPP), enabling the fabrication of sub-

micrometer features (**Figure 2A**).^[50] One strategy is to incorporate magnetic NPs into the precursors and polymerize the composite matrix by TPP. Another common strategy consists of fabricating hydrogel-based helical microstructures and later attaching magnetic NPs onto their surface.

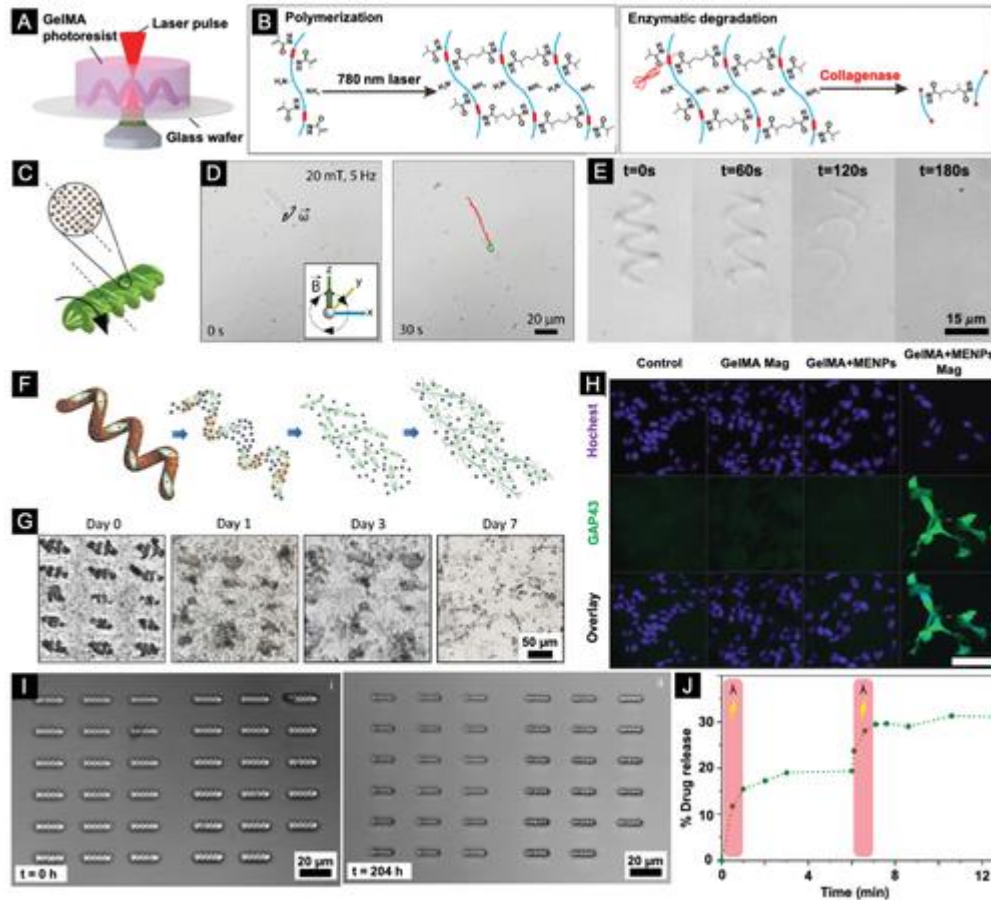


Figure 2

A) Schematic of the fabrication of GelMA microstructures by TPP. B) Illustration of polymerization (left) and enzymatic degradation (right) of GelMA. C) Schematic of alignment of magnetic NPs defining an easy axis normal to the helical axis of GelMA microswimmers, which allows their rotational motion under RMFs. (D) Image sequence of a GelMA microswimmer actuated under a RMF. C,D) Adapted with permission.^[50] Copyright 2019, American Chemical Society. E) Degradation of a GelMA helical microstructure in a collagenase solution (0.1 mg mL⁻¹). (A,B,E) Adapted with permission.^[52] Copyright 2018, Wiley-VCH. F) Illustration of the degradation process of cell-laden magnetoelectric GelMA microswimmers and induced neuronal differentiation under magnetic stimulation. G) Optical images showing the degradation process of the magnetoelectric GelMA microswimmers after they were cultured with SH-SY5Y cells for 0, 1, 3, and 7 days. H) Fluorescent images of SH-SY5Y cells cultured in different conditions. The nuclei were fluorescently stained in blue and the GAP 43 (protein related to neuronal growth) in green. Scale bar: 40 μ m. F–H) Adapted with permission.^[50] Copyright 2020, Wiley-VCH. I) Optical microscopy images of chitosan microswimmers treated with 15 μ g mL⁻¹ lysozyme, at $t = 0$ h (left) and $t = 204$ h (right). J) Smart dosing of DOX from the microswimmers triggered by NIR light. I,J) Adapted with permission.^[20] Copyright 2018, American Chemical Society.

Several reports have shown the fabrication of microrobots based on poly(ethylene glycol) diacrylate (PEGDA) hydrogel-based microstructures decorated with iron oxide NPs.^[51–52] PEGDA hydrogels are degraded in aqueous solutions by the hydrolytic cleavage of the ester bonds,^[53] yielding poly(acrylic

acid) (PAA) and poly(ethylene glycol) (PEG), both of which are harmless and commonly used in the biomedical field.^[54, 55] For instance, Peters et al. used this approach and cultured the microrobots with 3T3 fibroblast cells to demonstrate their drug delivery capabilities. Moreover, the microrobots were fully degraded in 1 M sodium hydroxide after 4 h and showed low cytotoxicity.^[51] Subsequently, Park et al. engineered similar microrobots and loaded them with the anticancer drug 5-fluorouracil. On the application of an alternating magnetic field (AMF), the microrobots released the drug and induced local hyperthermia, which considerably decreased the viability of the HCT116 cancer cells. The microrobots were fully degraded in 0.01 M sodium hydroxide after 30 h.^[52] Although the degradation of these microrobots was demonstrated in a basic medium to accelerate the hydrolytic reaction, they could also be degraded in physiological mediums, although at lower rates. To increase the biodegradability of microrobots, PEGDA was replaced by gelatin methacryloyl (GelMA) as a hydrogel precursor during the fabrication of helical microstructures.^[56-58] GelMA polymers are obtained by functionalizing gelatin, which is a polypeptide mixture of denatured and partially hydrolyzed collagen, with methacryloyl photo-reactive groups. These compounds can be naturally degraded in the body, since gelatin is known to be digested by proteases such as matrix metalloproteinase-2 (MMP-2) (Figure 2B).^[59, 60] For example, Ceylan et al. coated GelMA-based microstructures with iron oxide NPs and loaded them with dextran-fluorescein isothiocyanate (dextran-FITC) as the model drug. Due to the alignment of the magnetic NPs in the helical microstructures, the microrobots were effectively steered by a rotating magnetic field (RMF) (Figure 2C,D). They observed that the microrobots degradation rate and the subsequent drug release could be controlled by the MMP-2 concentration in the medium. Since there are some types of cancer with abnormally high MMP-2 concentrations,^[61] these microrobots could be of interest for tumor-targeted drug delivery applications.^[56] Pané and coworkers studied the degradation of the GelMA-based microrobots in the presence of either MMP-2 or protease-secreting cells, using HaCaT as a model. The microrobots were degraded after a few minutes using MMP-2 (Figure 2E), where the degradation rate was dependent on both the enzyme concentration and the microrobots' structural features. When the microrobots were incubated with HaCaT cells, the degradation was much slower, ca. 1 week, and cell viability was preserved. These results demonstrated the biocompatibility and biodegradability of the microrobots.^[57] In a subsequent study, the same group developed GelMA-based magnetoelectric helical microrobots by attaching cobalt ferrite-bismuth ferrite (CFO-BFO) magnetoelectric NPs for targeted cell delivery and in situ differentiation. Microrobots loaded with SH-SY5Y neuronal cells could be steered when RMF was applied. The microrobots were degraded after 7 days, which was attributed to the proteinases secreted by the SH-SY5Y cells (Figure 2F,G).^[58] Subsequently, the generated localized electric fields upon an AMF could induce differentiation of the SH-SY5Y cells (Figure 2F,H). These characteristics make magnetoelectric soft microrobots promising for cell therapies in nervous systems. However, the intracellular metabolism of CFO-BFO NPs and their long-term biocompatibility and bioresorbability still need to be investigated.^[62]

Gelatin-based hydrogels have been used in other ways to fabricate magnetic microrobots. For example, Kim et al. engineered a system of nested carriers made of DOX loaded PLGA MPs embedded in a gelatin-PVA-(magnetic NPs) hydrogel. In an in vitro experiment with Hep3B cells, the microrobots were decomposed thermally upon near-infrared (NIR) irradiation, releasing the magnetic NPs, which were retrieved with a magnet, and the DOX-PLGA MPs. The remaining materials provoked a significant decrease in cell viability after 12 h, as compared with DOX-free microrobots.

In addition to gelatin, other biodegradable hydrogels derived from natural compounds, such as alginate and chitosan, have also been used to develop magnetic microrobots. Alginate can be obtained from different algae and bacteria, and can be easily cross-linked with calcium to form hydrogels that can be selectively degraded in different temperature or pH conditions.^[63, 64] Hu et al. reported the fabrication of star-shaped MPs consistent with a mixture of alginate, PVA, DOX and iron oxide NPs. The microrobots demonstrated effective motion under a RMF and release of the drug in a slightly acidic medium. Interestingly, the microrobots were considerably degraded in the presence of amylase, an endogenous human enzyme, suggesting that alginate polymers could even be degraded by some human enzymes.^[65] In a similar approach, Rutkowski et al. engineered microcapsules made of alginate-calcium hydrogel, which were loaded with polyallylamine hydrochloride-rhodamine B isothiocyanate (PAH-RITC) and coated with iron oxide NPs. The microrobots were steered under a RMF, and the drug release was effectively triggered by ultrasound stimulation.^[66] Mair et al. encapsulated Au-Ni-Au nanorods into alginate sub-millimeter sized capsules, which were highly magnetized by aligning the nanorods. By applying a RMF, the capsules were able to roll over rough tissue surfaces and transport molecular payloads in vitro.^[67]

As mentioned above, other microrobots have been designed with a chitosan-based structure. Chitosan, which is obtained from the polysaccharide chitin, is naturally degraded by lysozyme, an enzyme widely present in the human body.^[68, 69] For instance, Bozuyuk et al. fabricated helical microrobots consisting of iron oxide NPs immersed in a chitosan matrix. The microswimmers were steered under a RMF and were partially degraded in the presence of lysozyme, whose concentration played a key role in the microrobots' degradation rate. However, the microrobots were not fully degraded even after 200 h (Figure 2I). By linking DOX to the microrobots surface by O-Nitrobenzyl photocleavable groups, the authors could trigger drug release by applying UV light (Figure 2J).^[70] Due to their slow degradation rates, in agreement with other related studies,^[71, 72] chitosan-based biodegradable robots may show potential for long-lasting biomedical applications.

Many research groups have designed magnetic microrobots with biological components. The biological materials can be naturally degraded in the body owing to their composition, resulting in a high interest in developing biodegradable medical microrobots with biological building blocks. In this context, some groups incorporated bacterial flagella into magnetic microrobots in order to enhance their propulsion ability. For instance, Shitanda et al. engineered magnetic nanorobots, consisting of

a Au-Ni-Au nanowire with a bacterial flagellum attached to one end. By applying a RMF, the nanorobots were propelled thanks to the flagellar motion induced by the rotation of the magnetic head, demonstrating the efficiency of flagella as a biodegradable constituent of magnetically-steered nanorobots.^[73] In other studies, bacterial flagella were replaced by DNA-based structures to propel microrobots. For example, Maier et al. decorated individual iron oxide MPs with DNA self-assembled nanotubes. On the application of a RMF, the microsystems were propelled similarly to flagellated bacteria, since the DNA-nanotubes behaved as flagella bundles that propelled the magnetic MPs (Figure 3).^[74]

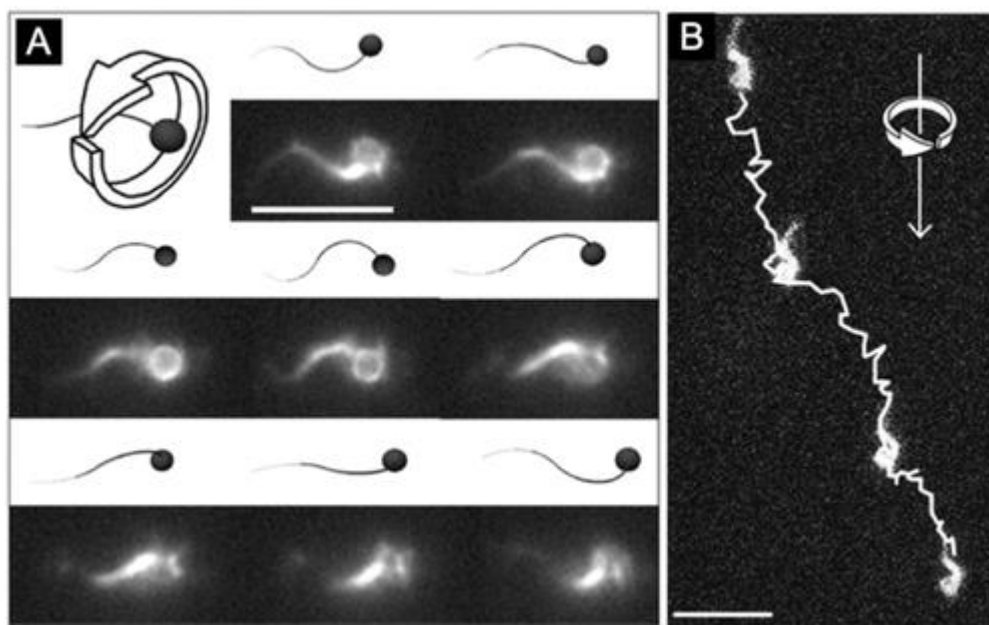


Figure 3
A) Schematic illustration and individual fluorescence microscopy images of a DNA-flagellated microrobot driven by a RMF. B) Tracking of a DNA-flagellated microrobot. Scale bars: 10 μm . A,B) Reproduced with permission.^[74] Copyright 2016, American Chemical Society.

Cell membranes can also be used to enhance the biodegradability and the in vivo performance of nanorobots. Following this idea, Li et al. fabricated Pd-Ni-Au helical nanorobots coated with platelet membranes. They tested the motion of the nanorobots under a RMF in different physiological media and observed that the platelet-based protection considerably increased the steering performance of the nanorobots. According to the authors, the platelet membranes avoided the adhesion of biomolecules that could hinder the nanorobots' motion. Moreover, the platelet-coated nanorobots were able to selectively bind bacterial toxins and platelet-adhering pathogens.^[75] Although this report did not focus on fully biodegradable nanorobots, it shows that platelet membranes might be a useful constituent for biodegradable small-scale robotics.

In many reports, the biological material was incorporated as the main structure of the magnetic microrobots. Recent studies have shown the potential of microrobots containing *Spirulina* microalgae as the structural core. These filamentous microalgae, with a helical shape and a length of a few hundred micrometers, can be easily magnetized by decorating them with

magnetic NPs, so that they can be maneuvered with a RMF in low Reynolds number regime. Due to their biological composition, they are naturally degraded in the physiological medium and are an attractive scaffold for biodegradable microrobots. In addition to their use as a food supplement, several studies have demonstrated their therapeutic efficacy with anti-viral, anti-bacterial and even anti-tumoral properties.^[76, 77] The majority of *Spirulina*-based magnetic microrobots are fabricated by dip-coating the microalgae in a suspension of iron oxide NPs in order to attach them to their surface (Figure 4A,B).^[26, 78-80] The effective motion of these microrobots under a RMF has been shown in different physiological media (Figure 4C),^[26] reaching relatively high speeds.^[80] The ability to load, transport and release cargos like small molecules or big biomacromolecules^[78, 79] has also been demonstrated. Furthermore, their high biocompatibility and biodegradability (with a degradation time of few days) have also been demonstrated in vitro (Figure 4D).^[26, 80] *Spirulina*-based microrobots have shown additional functionalities too. For example, Yan et al. demonstrated the outstanding in vivo imaging capabilities of these microrobots, which were used as contrast agents in mice for fluorescence and magnetic resonance imaging (MRI) (Figure 4E,F).^[26] The authors subsequently studied the drug delivery capabilities of the microrobots with different cargos; when releasing TGF- β 1 in the presence of hMSC cells, they observed the differentiation of the stem cells, demonstrating the conserved bioactivity of the growth factor after being transported by the microrobots.^[78] Wang et al. decorated the *Spirulina*-based microrobots with Pd-Au NPs and loaded them with DOX. When irradiated with NIR light in the presence of 769-P and EC109 tumoral cells, the microrobots produced local hyperthermia due to the photothermal properties of Pd-Au NPs. This led to the microrobots degradation and the subsequent DOX release, resulting in a combined chemophototherapy that drastically reduced the viability of the tumor cells. In addition to their antitumoral properties, this study demonstrated that the degradation of *Spirulina*-based microrobots may be triggered by stimuli like local temperature changes.^[79] Liu et al. demonstrated the electrostimulation capabilities of *Spirulina*-based microrobots. The microrobots were decorated with barium titanate NPs on their surface, and then cultured with PC12 neuron-like stem cells. Under ultrasound stimulation, the piezoelectric barium titanate NPs generated localized electric fields that induced the neuronal differentiation of the surrounding cells, and no cytotoxic effects were observed.^[80]

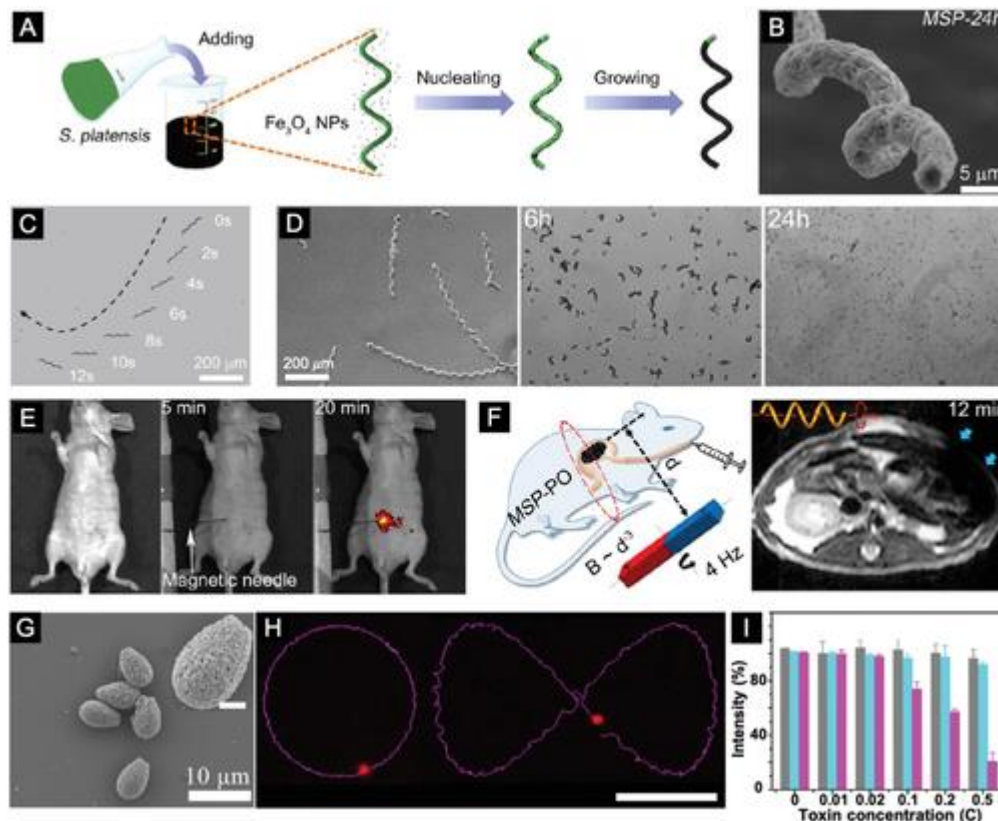


Figure 4

A) Schematic of the dip-coating process of *Spirulina* in a suspension of iron oxide NPs. B) An SEM image of a *Spirulina* microrobot. C) A time-lapse image of the controlled locomotion of a microrobot under a RMF. D) Degradation of microrobots in a 37 $^\circ\text{C}$ DPBS solution. E) Fluorescence of microrobots in the intraperitoneal cavity of mice at different residence times. A magnetic needle was used to move and concentrate the microrobots in a specific area. F) Scheme of MRI of a rat's stomach after administration of microrobots (left). Microrobots were injected subcutaneously and subjected to magnetic actuation and steering before MRI across the rat's stomach (right). A–F) Adapted with permission.^[26] Copyright 2017, AAAS. G) An SEM image of spore microrobots after coating with iron oxide NPs and carbon dots. Scale bar (inset): 2 μm . H) Trajectories of the navigation of the spore microrobots under a RMF. Scale bar: 100 μm . I) Detection of *Clostridium difficile* toxin in stool samples. Difference in fluorescence intensity of mobile microrobots in patient's sample (pink bars) versus normal sample (grey bars) and versus static microrobots (blue bars), for different toxin concentrations. The authors defined $C = 8.66 \text{ ng mL}^{-1}$. The fluorescence decay is directly correlated to the attachment of toxins. G–I) Adapted with permission.^[81] Copyright 2019, AAAS.

Other interesting biomaterials for the microrobot structure are spores obtained from plants or fungi. For example, *Ganoderma lucidum* spores, which have an oval shape and are around 5 μm in size, possess a large hollow cavity and a rough, porous surface. These properties, together with their intrinsic biodegradability and low cost, make these spores ideal for drug delivery purposes. Zhang et al. fabricated spore-based microrobots by immersing *G. lucidum* spores in a suspension of iron oxide NPs and conjugating the magnetic spores with carbon dots (Figure 4G). Under RMF, the microrobots showed effective motion in different media such as water, PBS, stomach mucus and intestinal mucus (Figure 4H). The microrobots demonstrated excellent toxin detection capabilities (Figure 4I), owing to the active motion and high surface area of the magnetic spores, combined with the inherent fluorescence and affinity of carbon dots toward specific toxins.^[81]

A summary of all the aforementioned magnetically driven biodegradable micro- and nanorobots is listed in **Table 1**.

Table 1. Magnetically driven biodegradable micro- and nanorobots (biodegradable components are marked in **bold**)

Substrate/chassis	Motile components	Shape (Size)	Functionality/application (functional part)	Degradability assay	Ref.
Fe		Helical (25 × 100 μm)	–	acidic, 20 min	[41]
PLGA	Fe-Co NPs	Spherical (60 μm)	In vivo chemoembolization (DOX)	nd	[46, 47]
PLGA	Fe MPs	2D shapes (240–600 μm)	Drug release	pH 7.4, 37 °C, 7 weeks	[48]
PEGDA	Iron oxide NPs	Helical (5–40 × 30–120 μm)	Drug release	basic, 4 h	[51]
			AMF-triggered drug release and hyperthermia (Iron oxide NPs)	basic, 30 h	[52]
GelMA	Iron oxide NPs	Helical (5–20 × 20–50 μm)	Enzyme-triggered drug release	MMP-2, pH 7.4, 37 °C, 5 days	[56]
			–	cell-secreted proteases, pH 7.4, 37 °C, 1 week	[57]
	CFO-BFO NPs		Cell delivery and electrostimulation (CFO-BFO NPs)	cell-secreted proteases, pH 7.4, 37 °C, 1 week	[58]

Substrate/chassis	Motile components	Shape (Size)	Functionality/application (functional part)	Degradability assay	Ref.
Alginate	Iron oxide NPs	Star-like (20 µm)	pH-triggered drug release	amylase, pH: 7.4, time: 24 h	[65]
		Spherical (50–100 µm)	Ultrasound-triggered drug release	nd	[66]
	Au-Ni-Au nanorods	Spherical (800 µm)	Drug release	nd	[67]
Chitosan	Iron oxide NPs	Helical (5 × 20 µm)	Light-triggered drug release (photocleavable linker)	lysozyme, pH 7.4, 37 °C, > 9 days	[70]
Au-Ni-Au nanowires + bacterial flagella		Head (200 nm × 5 µm) + tail (15 µm)	–	nd	[73]
Iron oxide MPs + DNA nanotubes		Head (1 µm) + tail (10 µm)	–	nd	[74]
Pd-Ni-Au nanohelices		Helical (400 nm × 5 µm)	Biodetoxification (platelet membranes)	nd	[75]
Spirulina	Iron oxide NPs	Helical (10–50 × 100–200 µm)	In vivo fluorescence (<i>Spirulina</i>) and MRI (iron oxide NPs)	pH 7.4, 37 °C, > 24 h	[26]
			Drug transport and release	nd	[78]

Substrate/chassis	Motile components	Shape (Size)	Functionality/application (functional part)	Degradability assay	Ref.
			Light-triggered chemo-phototherapy (Pd-Au NPs, DOX)	NIR laser, 20 min	[79]
			Piezoelectric cell differentiation (barium titanate NPs)	pH 7.4, 37 °C, 5 days	[80]
Spores	Iron oxide NPs	Oval (5 µm)	Toxin detection (carbon dots)	nd	[81]

3 Light/Ultrasound-Driven Biodegradable Small-Scale Swimmers

Micro- and nanorobots actuated with light or ultrasound are found in a significant amount of literature within the field, however only a few are biodegradable.^[82, 83] Light-driven nanorobots make use of photocatalytic materials such as zinc oxide, which is biocompatible and biodegradable,^[84] to enhance Pt catalysis of hydrogen peroxide (Figure 5A,B),^[85] or to propel by electrophoretic gradients.^[86] Many other light-driven nanorobots integrate Au coatings or NPs, which absorb NIR light and generate thermal gradients. These thermal gradients are responsible for the movement of the robots. A simple biodegradable example is Au-deposited Janus mesoporous silica NPs.^[87] Another example is the chitosan-heparin capsule partially coated with Au and fully covered with red blood cell (RBC) membranes (Figure 5C); when irradiated with NIR light, the Au cap generates a thermal gradient that drives the motion of the microrobots (Figure 5D). This localized photothermal effect, combined with the anticoagulant function of heparin, was used to dissolve fibrinogen thrombus in vitro (Figure 5E). Moreover, coating the microrobots with RBC membranes prevented biofouling and helped to preserve their motion in the cell culture medium, serum and blood.^[88]

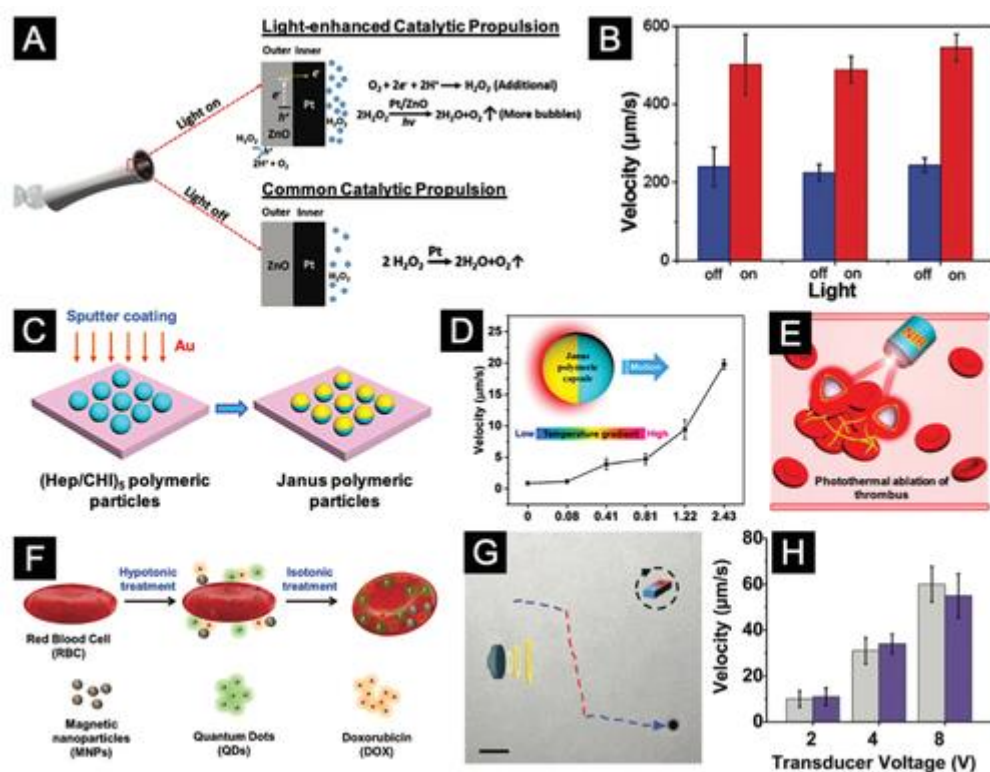


Figure 5

Light and ultrasound-driven micro- and nanorobots. A) A scheme of ZnO–Pt microrobot's propulsion mechanism in the presence and absence of UV light. B) The velocity of ZnO–Pt microrobots under UV light and without UV light. A,B) Adapted with permission.^[85] Copyright 2017, The Royal Society of Chemistry. C) Fabrication of (heparin/chitosan)-Au light-driven biodegradable microrobots, which are subsequently covered with RBC membrane. D) The velocity of (heparin/chitosan)-Au microrobots as a function of laser power. The inset image is the schematic representation of the movement of the microrobots driven by the NIR laser. E) Schematic illustration of photothermal ablation of thrombus. C–E) Adapted with permission.^[86] Copyright 2018, American Chemical Society. F) Preparation of ultrasound-driven biodegradable microrobots based on RBC cells loaded with quantum dots imaging nanocrystals, DOX and iron oxide NPs through a hypotonic dilution-based encapsulation method. G) RBC-based microrobot's trajectory under an ultrasound field (voltage of 4 V and frequency of 2.4 MHz) oriented with an external magnetic field provided by manually rotating a handheld magnet. Scale bar: 20 μm . H) The velocity of RBC robots without payloads (grey bars) and multicargo-loaded RBC robots (purple bars) using different ultrasound voltages at a frequency of 2.4 MHz. F–H) Reproduced with permission.^[83] Copyright 2015, The Royal Society of Chemistry.

Ultrasound can also be used to propel micro- and nanorobots. Wang et al. were the first to show that metallic microrods within the nodal plane of acoustic standing waves propelled ballistically in the axial direction, as opposed to polymeric rods of similar size and shape. It was also suggested that the concave ending of the rods is crucial to promote their directional motion, although the mechanism behind this is not yet well understood.^[89, 90] These findings have restricted most acoustic robots to asymmetric metallic structures, typically made of Au, which are not biodegradable themselves. However, Au nanorods covered with RBC or platelet membranes are also worth mentioning, given their partial biodegradability. These nanorobots could trap toxins (α -toxin and melittin) and pathogens while preventing biofouling.^[91, 92] For a more biodegradable example, Wu et al. fabricated acoustic microrobots based on RBCs loaded with DOX and iron oxide NPs (Figure 5F–H). The authors

suggested that the encapsulated and aggregated magnetic NPs provided sufficient density to allow ultrasound propulsion.^[93]

For reference, a summary of biodegradable micro- and nanorobots driven by light or ultrasound is presented in **Table 2**.

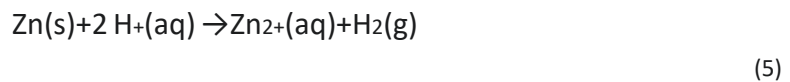
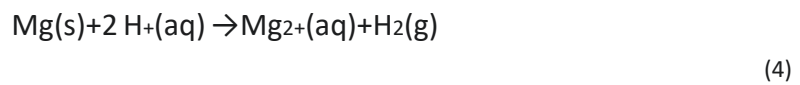
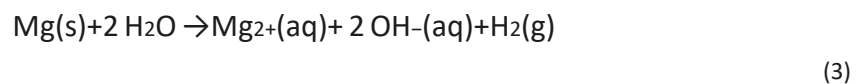
Table 2. Light/ultrasound-driven biodegradable micro- and nanorobots (biodegradable components are marked in **bold**)

	Substrate/chassis		Motile components	Shape (Size)	Functionality/application (functional part)	Degradability assay	Ref.
Light	Pt-ZnO		Pt layer	Tubular (3 μm × 20 μm)	—	nd	[85]
	ZnO		Au layer	Rod-like (1.5 μm × 3.4 μm)	Cargo transport	nd	[86]
	Mesoporous Janus NPs	silica	Au layer	Spherical (50–120 nm)	—	nd	[87]
Acoustic	Chitosan-heparin		Au layer	Spherical (5 μm)	—	pH 7.4, 37 °C, 24 h	[88]
	Au			Rod-like (400 nm × 3 μm)	Toxin and pathogen binding (RBC and platelet membranes)	nd	[91, 92]
	RBC		Iron oxide NPs	RBC (6–8 μm)	Magnetic steering (iron oxide NPs), fluorescence (quantum dots), drug release	nd	[93]

4 Chemically Driven Biodegradable Small-Scale Swimmers

Chemically driven small-scale swimmers, which are also termed micro- and nanomotors, are propelled by reactions triggered by chemical species existing in their swimming environment. Three propulsion mechanisms have been identified for these micro- and nanoswimmers: a) bubble propulsion, where gas bubbles generated by the chemical reactions impart momentum to the micro- and nanomotors when they are asymmetrically released from the motor's scaffold; b) self-electrophoresis propulsion, where the migration of protons and electrons of bimetallic micromotors contributes to an electrical field that propels the charged micromotors forward; and c) self-diffusiophoresis propulsion, where the products of the chemical reaction generate a concentration gradient around the swimmer that leads to its locomotion. For a detailed explanation of these mechanisms, we refer the reader to earlier reviews.^[18, 94, 95] The majority of chemically driven micro- and nanomotors are usually propelled by chemical fuels such as hydrogen peroxide or hydrazine. However, these toxic fuels hinder the applications of these small-scale motors in the biomedical field.

Most chemical micro- and nanoswimmers are built either with metals such as platinum, rhodium, or ruthenium, which are not biodegradable, or they decompose into cytotoxic ions.^[96] However, micro- and nanomotors based on metals with biocompatible characteristics, such as zinc or magnesium, have gained attention in the last decade. Note that although these elements are vital for several biological functions,^[97, 98] high level exposure of these metals can cause adverse effects.^[99, 100] Mg-based micromotors can be propelled in an aqueous or acidic medium, due to the generation of hydrogen bubbles (Equations (3) and (4)). The propulsion of Zn-based micromotors relies on the same mechanism, but in this case hydrogen bubbles are only produced in an acidic medium (Equation (5)). Note that the self-propulsion of micro- and nanomotors based on Mg or Zn in biological medium also implies their degradation, meaning that these devices are inherently biodegradable but they have limited propulsion and action time.^[101-103]



Regarding Mg micro- and nanomotors, most of the reported cases consist of Janus MPs with a Mg core and a metal or metal oxide layer (Au,^[101, 102, 104] Pt,^[105, 106] TiO₂,^[107-109] ZnO,^[110] Si^[110]), which enhances their locomotion capabilities by galvanic corrosion.^[101] Another approach used in literature consists in incorporating Mg MPs in the inner cavity of metal-polymer microtubes.^[111] The efficient self-propulsion of Mg-based micromotors was demonstrated in a wide variety of media, such as water,^[101, 105] blood plasma,^[104, 106] gastric acid,^[102] or intestinal fluid,^[109, 111] achieving velocities between 30 and 100 $\mu\text{m s}^{-1}$ (Figure 6A,B). Moreover, they also showed to be useful for different applications. For example, Guan and coworkers proved the effective loading, transport and

temperature-triggered release of fluorescein isothiocyanate (FITC) using Mg micromotors coated with a thermo-responsive poly(N-isopropylacrylamide) (PNIPAM) hydrogel.^[106] Wang and coworkers demonstrated the effective detoxification properties of Mg micromotors coated with RBC membranes. Being “camouflaged” as RBCs, the micromotors were able to remove two different compounds (a-toxin and methyl-paraoxon) in an albumin-rich medium.^[104] Additionally, the same group also demonstrated other relevant in vivo applications of Mg micromotors. Using micromotors with a pH-responsive polymer as enteric coating, they showed interesting outcomes in in vivo studies with mice: (i) the self-propulsion of the micromotors significantly increased the retention of cargo in the site of interest;^[102, 107, 108, 111] (ii) the positioning of the micromotors inside the gastrointestinal tract could be controlled by adjusting the thickness of the enteric coating (Figure 6C,D);^[111] (iii) the Mg-H⁺ redox reaction temporarily neutralized the gastric acid in the stomach, enabling effective treatments without the need for the commonly used proton-pump inhibitors;^[102, 107] and (iv) drug-loaded micromotors demonstrated therapeutic efficacy against a bacterial infection^[107] and anemia (Figure 6E).^[109] Interestingly, they also proved the increased retention of Mg micromotors in mice stomach by encapsulating them in excipient-containing pills, presenting a further step towards the translation of these biodegradable micromotors into clinical applications.^[108]

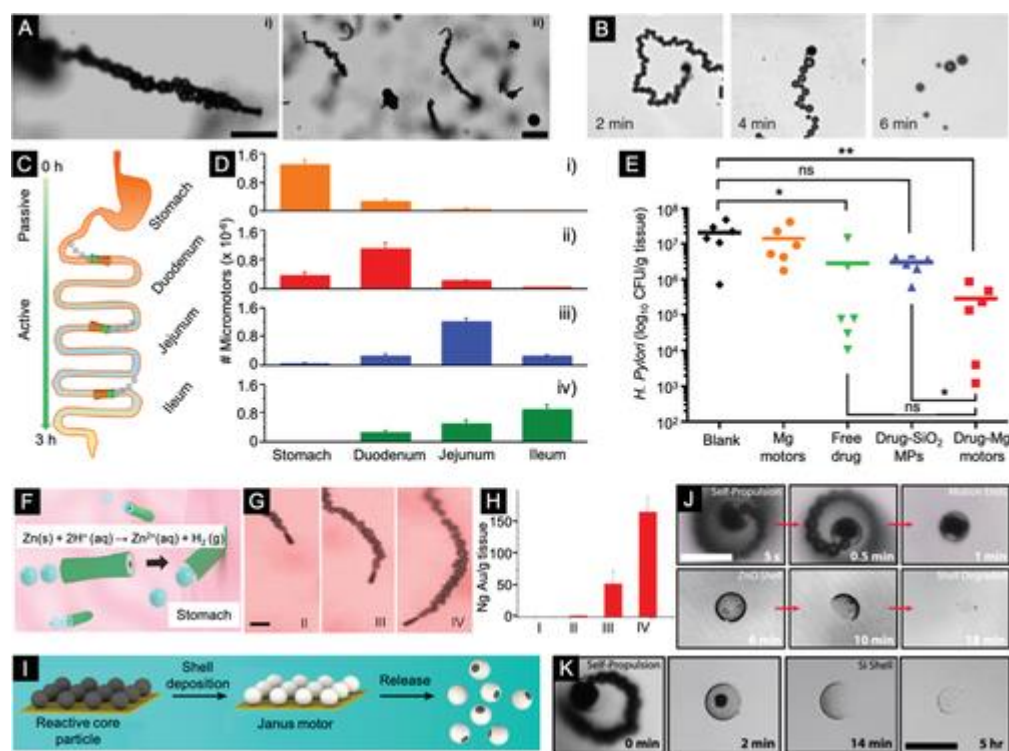


Figure 6

A) Propulsion snapshot of a single (left) and multiple (right) Mg-based micromotors in intestinal fluid. Scale bars: 40 μ m. B) Time-lapse images of the propulsion of drug-loaded Mg micromotors in simulated gastric fluid. C) Schematic representation of the localization and retention of Mg micromotors in the stomach and gastrointestinal tract. D) In vivo selective retention of Mg micromotors. Inductively coupled plasma-mass spectrometry analysis of the number of micromotors with different enteric coating thickness retained in mice stomach, duodenum, jejunum and ileum 6 h after oral administration. i) no coating, ii) thin coating, iii) medium coating, iv) thick coating. A,C,D) Adapted with permission.^[111] Copyright 2016, American Chemical Society. E) In vivo antibacterial

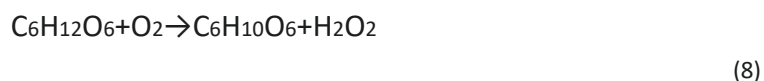
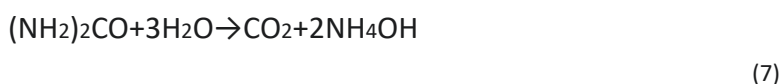
therapeutic efficacy of drug-loaded Mg micromotors. Quantification of *Helicobacter pylori* burden in mice stomach treated with water (black), bare Mg micromotors (orange), free drug (green), drug-loaded silica MPs (blue) and drug-loaded Mg micromotors. B,E) Adapted under the terms of the CC-BY 4.0 license.^[107] Copyright 2017, The Authors, published by Springer Nature. F) Schematic of the propulsion and tissue penetration of Zn-based micromotors in the stomach. G) Time-lapse images of the propulsion of Zn micromotors in gastric acid at 37 °C. Scale bar: 20 µm. H) In vivo cargo delivery with Zn micromotors. Inductively coupled plasma-mass spectrometry analysis of the amount of Au retained in the stomach tissues of mice after oral administration of different samples: I) blank, II) Zn micromotors, III) Au NPs, and IV) Zn micromotors loaded with Au NPs. F–H). Adapted with permission.^[124] Copyright 2014, American Chemical Society. I) Schematic illustration of the fabrication of Janus micromotors with a Mg or Zn core: particles were spread on a glass substrate followed by sputtering of shell materials and release. J) Time-lapse images of the motion and degradation of a Mg-ZnO micromotor in 0.5 M sodium bicarbonate solution. Upper row: self-propulsion stage (5, 30, 60 s, from left to right). Lower row: degradation stage (6 min, 10 min, 18 min). Scale bar: 40 µm. K) Time-lapse images of the motion and degradation of a Mg-Si micromotor in a 0.5 M sodium bicarbonate solution. Scale bar: 40 µm. I–K) Adapted with permission.^[110] Copyright 2016, American Chemical Society.

To date, only a few studies have been conducted with Zn-based micromotors. The majority of reported Zn micromotors consist of microtubes with a Zn core and a polymeric shell,^[24, 103, 112] although recently Janus MPs^[110] and double-conical microstructures^[113] have also been investigated. Wang's group reported the first Zn micromotors, which demonstrated effective self-propulsion^[103, 113] and drug delivery capabilities^[113] in highly acidic environments; however, since they were only active at an extremely low pH, they lacked interest for biomedical applications. In subsequent studies, the motion of Zn micromotors in gastric acid environments was demonstrated, and in vivo experiments proved their ability to effectively deliver drugs in the stomach with no toxicity signs and with an enhanced drug retention due to their self-propulsion (Figure 6F–H).^[24, 112]

Interestingly, some Mg or Zn micromotors with fully biodegradable structures have been reported. Chen et al. fabricated Janus MPs with Mg-ZnO, Mg-Si and Mg-Fe compositions, and single-phase Zn MPs, which showed effective motion in acidic or aqueous media, achieving remarkable speeds and propulsion times (Figure 6I–K). Their degradation time was controlled by changing their composition; for example, Mg-ZnO micromotors were degraded after 18 min (Figure 6J), whereas Mg-Si micromotors were degraded after 5 h (Figure 6K). This tuneability of the degradation time may be of interest for clinical applications requiring different action times.^[110] Zhou et al. developed Zn-Fe-poly(aspartic acid) tubular micromotors that demonstrated increased drug retention in mice stomach with no toxic effects. After completing their therapeutic tasks, the micromotors were fully degraded, since Mg and Fe are dissolved in gastric acid and poly(aspartic acid) is known to be digested by proteases present in the digestive tract.^[112]

Silica-based micro- and nanomotors have also been extensively studied. Despite widespread misconceptions, silica is soluble in aqueous media, as it undergoes hydrolysis to form silicic acid, which is non-toxic and can be resorbed by renal excretion.^[114] In biological conditions, porous silica NPs degrade in days-weeks, while non-porous silica may take more time given its lower surface-area ratio.^[115] Moreover, the fabrication of silica particles of different sizes and shapes is simple and well documented, as well as their surface functionalization methods. Initially, most silica micro- and nanomotors used hydrogen peroxide as fuel. Silica-Pt Janus micro- and nanomotors could self-propel through the conversion of hydrogen peroxide into water and oxygen (Equation (6)).^[116] However, the

limited bioavailability and the toxicity of hydrogen peroxide encouraged researchers to find new solutions, for example, the use of more biocompatible propelling mechanisms. In this vein, Sánchez and coworkers developed silica nanomotors functionalized with urease, where the propulsion was accomplished by the enzymatic conversion of urea to ammonia and carbon dioxide (Equation (7)).^[117, 118] In this approach, not only the biocompatibility of the device was improved but also the biodegradability, as urease is an enzyme and is therefore inherently biodegradable. Interestingly, they observed that due to the stochastic patchiness of the functionalization, they did not have to design an asymmetry in the structure of the nanomotors to achieve a directional motion.^[119] In a cell viability assay with HeLa cells, DOX-loaded urease-powered nanomotors were twice as cytotoxic as drug-free nanomotors. In the absence of urea, the cytotoxicity of drug-loaded and drug-free nanomotors was similar. They attributed these results to the improved DOX release induced by motion and the ammonia generated from urea decomposition^[120]



As with magnetically driven micro- and nanorobots, chemically driven micro- and nanomotors can also integrate biodegradable organic materials into their skeleton or scaffold. Polymersomes, for example, are a class of artificial vesicles made of amphiphilic block copolymers, which can be converted into the so-called stomatocytes through dialysis-driven artificial endocytosis. Stomatocytes are polymersomes with an almost-closed bowl-shape that can entrap catalytic agents in their nanocavities to serve as self-propelled micro- and nanomotors. These stomatocytes were initially fabricated using a block copolymer of PEG and polystyrene (PS) (PEG-b-PS) and were therefore not biodegradable.^[121] However, Tu et al. fabricated stomatocytes from a mixture of PEG-b-PCL and PEG-b-PS, with Pt NPs entrapped in the nanocavities and DOX loaded in the lumen. PCL proved to be critical in the biodegradability of the nanomotors and their subsequent drug release. In fact, as shown from an in vitro experiment with HeLa cells, DOX could diffuse out of stomatocytes integrating PCL, but stayed confined in stomatocytes without PCL.^[122] In terms of biodegradability, similar results were obtained for stomatocytes in which the PEG and PS block were linked with redox-sensitive disulfide bonds (PEG-SS-PS). In this case, disulfide bonds could be cleaved by glutathione, a redox modulator present in intracellular compartments that is overexpressed in cancer cells, promoting drug release and the degradation of the nanomotor.^[123] Following this work, Toebes et al. developed biodegradable catalase (Cat)-propelled tubular nano-sized polymersomes made of PEG-b-PDLLA and proved their drug loading capabilities.^[124] They later improved their own concept by fabricating PEG-b-PDLLA nano-sized stomatocytes and selectively functionalizing their inner surface with glucose oxidase (GOx) and Cat, and their outer surface with a dye or Au NPs. Thanks to the incorporation of the GOx-Cat tandem, the nanomotors were fueled by glucose, an abundant

bioavailable molecule (Equation (8)); and hydrogen peroxide was only produced as a by-product which was quickly decomposed by Cat.^[125]

In the search for more biodegradable approaches, other groups have fabricated chemically driven micromotors via layer-by-layer (LbL) assembly of biopolymers. This fabrication method relies on the alternating adsorption of anionic and cationic polymer layers on a porous template (**Figure 7A**). In this regard, He and coworkers fabricated micromotors based on a LbL assembly of chitosan (positively charged) and alginate (negatively charged). Such micromotors, propelled by hydrogen peroxide and steered with magnetic fields, were used in vitro to trap, transport and kill specific HeLa cells (Figure **7B**). Their therapeutic effect was realised through the incorporation of DOX, whose release was triggered with low-frequency ultrasound, as the alginate-chitosan multilayer degradation was accelerated.^[126, 127] The group also developed similar micromotors made of alternating poly(L-lysine) (PLL) (positively charged) and bovine serum albumin (BSA) (negatively charged), and filled with a mixture of gelatin, Cat, DOX, magnetic NPs and Au NPs. DOX release was accomplished upon irradiation with NIR light so that the photothermal effect caused the Au NPs to heat and melt the gelatin matrix (Figure **7C**). Furthermore, the micromotors could be degraded after several days of enzymatic treatment with α -chymotrypsin (Figure **7D**).^[128] Similarly, Komatsu's group developed biodegradable micromotors with alternating poly(L-arginine) (PLA) (positively charged) and human serum albumin (HSA) (negatively charged) as their structural materials. PLA can be degraded by trypsin,^[129] a peptidase naturally present in our bodies, and HSA is known to be degraded by all tissues, in particular muscle, liver and kidney.^[130] The authors fabricated three kinds of micromotors, whose inner surface was functionalized with Pt, Cat and urease, respectively, to propel them in solutions of hydrogen peroxide or urea (Figure **7E**). Given the excellent biodegradability of PLA and HSA, the micromotors were fully degraded after 120 min in a solution of a cocktail of proteases (Pronase) at pH 7.4 and 37 °C, or after 6 h at pH 3, leaving only the Pt NPs.^[131-133]

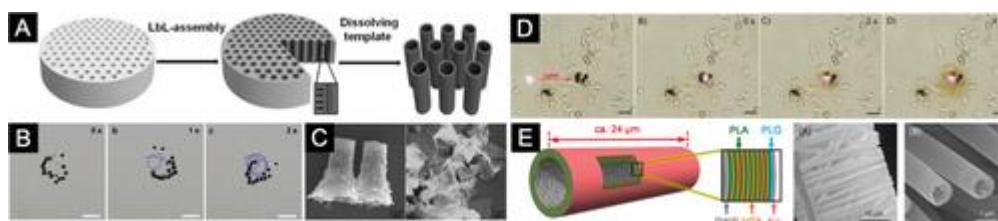


Figure 7

Micromotors fabricated by LbL. A) Scheme of the fabrication of micromotors via the LbL method. Black dots and vertical stripes (see expansion) represent Pt NPs and polyelectrolyte multilayers, respectively. Reproduced with permission.^[126] Copyright 2013, Wiley-VCH. B) Time-lapse images of chitosan-alginate micromotors transporting a single HeLa cell in a circular trajectory. Scale bar: 50 μ m. Used with permission from Hu et al. 2018.^[127] Copyright 2018, Wiley-VCH. C) Time-lapse images of triggering the DOX release from the PLL/BSA motors loaded with DOX-CAT-AuNPs-gelatin under NIR irradiation. The purple spot shows the NIR laser, whereas the brown solution indicates the DOX released from micromotors. Scale bar: 20 μ m. D) SEM images of the PLL/BSA motors loaded with DOX-CAT-AuNPs-gelatin, before (left) and after (right) incubation with the α -chymotrypsin solution. C,D) Adapted with permission.^[128] Copyright 2014, American Chemical Society. E) Schematic

illustration of a (PLA/HSA)-Pt micromotor (left), and the corresponding SEM (middle) and TEM (right) images. Adapted with permission.^[133] Copyright 2019, American Chemical Society.

Other micromotors are worth mentioning given their biodegradability and potential application. For instance, a microfluidic device was used to form chitosan-glutaraldehyde microcapsules asymmetrically loaded with a patch of core-shell Fe–Pt NPs (**Figure 8A**). These micromotors, fueled by hydrogen peroxide and steered by magnetic fields, could transport and release similar non-magnetic MPs, thus suggesting their potential application as a biodegradable^[134] and low-cost drug delivery platform.^[135] In a different approach, micromotors were fabricated by embedding cucurbit[6]uril-conjugated hyaluronate nanogels in Pt-coated calcium carbonate MPs. Hyaluronate is a naturally occurring biodegradable and biocompatible glycosaminoglycan polysaccharide that is highly present in the human body. It can be degraded by free radicals and lysozymes.^[63] When the micromotors were incubated with MDA-MB 231 cells at pH 6.5, simulating the microenvironment of a tumor, the acidic environment caused calcium carbonate to decompose and to release the embedded nanogels. The nanogels were then uptaken by the cancer cells via hyaluronate receptor-mediated endocytosis, and could subsequently degrade and release their cargo drugs (Figure 8B). It is noteworthy that these micromotors reached an encapsulation efficiency of 65% thanks to the host-guest interaction provided by cucurbit[6]uril, and that their cytotoxicity was negligible up to a concentration of 1 mg mL⁻¹.^[136]

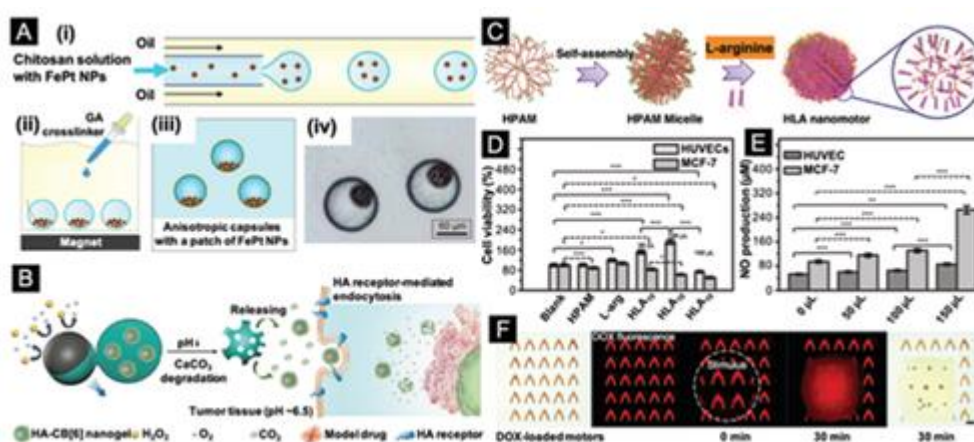


Figure 8

A) Fabrication steps of chitosan-glutaraldehyde micromotors: i) generation of chitosan droplets with Fe–Pt NPs using a microfluidic device, ii) aggregation of magnetic NPs with a magnet and the addition of glutaraldehyde, iii) washing and placement in water. (iv) close-up of the final capsules. Scale bar: 60 μm . Adapted with permission.^[135] Copyright 2016, American Chemical Society. B) Intracellular delivery of model drugs loaded in the Pt/CaCO₃/HA-CB[6] nanomotors by the dual stimuli-responsive targeting effect: the pH-responsive degradation of calcium carbonate in the acidic tumor environment and the cancer cell targeting capability of HA nanogels via HA receptors on the cancer cells. Adapted with permission.^[136] Copyright 2019, Wiley-VCH. C) Scheme of the formation of an HPAM/(L-arginine) (HLA) nanomotor. D) Cell viability results of HLA nanomotors with HUVECs and MCF-7 cells. E) Nitric oxide production amount during the co-culture of different amounts of HLA nanomotors with HUVECs and MCF-7 cells for 4 h. C–E) Adapted under the terms of the CC-BY 4.0 license.^[137] Copyright 2019, The Authors, published by Springer Nature. F) Degradation of micromotors based on a squid ring teeth protein upon addition of diluted acetic acid and subsequent

release of DOX. Scale bar: 500 μm . Adapted under the terms of the CC-BY 4.0 license.^[139] Copyright 2019, The Authors, published by Springer Nature.

Micro- and nanomotors that carry the fuel within their structure also show potential. Having one of their components consumed over time is advantageous in terms of biodegradability, however their propulsion times are limited to the amount of fuel they can carry. Wan et al. fabricated nanomotors based on hyperbranched polyamide (HPAM) decorated with L-arginine (Figure 8C). Conversion of L-arginine to nitric oxide by nitric oxide synthase and other ROS could drive the motion of these nanomotors in tumor-like environments, where the concentration of ROS is known to be higher. In fact, incubation of the nanomotors with HUVEC and MCF-7 cells promoted their proliferation and death, respectively. The proliferative effect was ascribed solely to L-arginine, while the cytotoxic effect was attributed to the increased levels of nitric oxide due to a higher ROS concentration in MCF-7 cells (Figure 8D,E). Furthermore, the authors enhanced the biodegradability by fabricating equivalent nanomotors with chitosan or PLL instead of HPAM.^[137] In a very different approach, Penafresch et al. fabricated biodegradable micromotors based on a squid ring teeth protein and propelled by Marangoni flows in an air-liquid interface. These micromotors integrated DOX and hexafluoroisopropanol (HFIP), a metabolite of sevoflurane, which is an FDA approved anesthetic. HFIP acted as a fuel, generating Marangoni flows as it was released from the protein matrix and driving the micromotors to regions with higher surface tension.^[138] Drug release and full degradation of the micromotors was demonstrated to occur within 30 min in acidic conditions (Figure 8F). This was attributed to the disruption of β -sheets that acted as crosslinkers.^[139]

The characteristics of the aforementioned chemically driven biodegradable micro- and nanomotors are summarised in Table 3.

Table 3. Chemically driven biodegradable micro- and nanomotors (biodegradable components are marked in **bold**)

Substrate/chassis	Motile components	Shape (Size)	Functionality/application (functional part)	Degradability assay	Ref.
Metallic Janus MPs	Mg or Zn MPs	Spherical (20–50 μm)	Detoxification (RBC membrane)	nd	[104]
			Temperature-triggered drug release (PNIPAM hydrogel)	nd	[106]
			In vivo stomach-targeted drug delivery	nd	[102, 107–109]

Substrate/chassis		Motile components	Shape (Size)	Functionality/application (functional part)	Degradability assay	Ref.
Polymeric microtubes				In vivo antibacterial therapy (antibiotic payload)	nd	[107]
				In vivo therapy against anemia (Fe/Se payload)	nd	[109]
				—	nd	[101, 105, 110]
				In vivo stomach-targeted drug delivery	nd	[24, 111, 112]
				—	nd	[103]
Zn			Tubular (2–10 × 10–20 µm)	Cargo transport and release	nd	[113]
Mesoporous Janus NPs	silica	Pt layer	Spherical (65 nm)	Drug release	nd	[116]
		Urease, GOx	Janus spherical (400 nm)	—	nd	[117]
Hollow silica MPs		Urease, Acetylcholinesterase	Spherical (2 µm)	—	nd	[118]
Core-shell mesoporous silica NPs		Urease	Spherical (400 nm)	Drug release	nd	[120]

Substrate/chassis	Motile components	Shape (Size)	Functionality/application (functional part)	Degradability assay	Ref.
PEG-b-PCL / PEG-b-PS mixture	Pt NPs	Vesicular (350 nm)	Drug release	pH 1, 12 h	[122]
PEG-SS-PS			Redox-triggered drug release (disulfide bond)	nd	[123]
PEG-b-PDLLA	Cat	Tubular (150 × 900 nm)	Drug release	nd	[124]
	GOx, Cat	Vesicular (250 nm)	Drug release	nd	[125]
Chitosan-alginate	Pt NPs	Tubular (600 nm × 10 µm)	Magnetic steering (iron oxide NPs), ultrasound-triggered drug release	nd	[126]
		Tubular (2–4 × 30–40 µm)	Cell transport	nd	[127]
PLL-BSA-gelatin	Cat	Tubular (5 × 10 µm)	Magnetic steering (iron oxide NPs), light-triggered drug release (Au NPs)	α-chymotrypsin, pH 7.4, 20 °C, 12 h	[128]
PLA-HSA	Cat	Tubular (1 × 24 µm)	–	Pronase, pH 3, 2 h	[131]
	Urease		–	Pronase, pH 3, 37 °C, 2 h	[132]

Substrate/chassis	Motile components	Shape (Size)	Functionality/application (functional part)	Degradability assay	Ref.
	Pt NPs		Specific molecular trapping (avidinated surface)	Pronase, pH 7.5, 37 °C, 2 h	[133]
Chitosan-glutaraldehyde	Fe–Pt NPs	Spherical (150 µm)	Cargo transport	nd	[135]
CaCO ₃ /HA-CB[6]	Pt layer	Spherical (1 µm)	Drug release	pH 6.5	[136]
HPAM, chitosan, PLL	L-arginine	Spherical (100–400 nm)	Drug release	nd	[137]
SQR protein	HFIP	V-like (10 µm–10 mm)	Drug release	acidic, 30 min	[139]

5 Hybrid Biodegradable Small-Scale Swimmers Based on Microorganisms

In the last decades, special interest has been given to small-scale swimmers that are propelled by living microorganisms. Any biological entity is inherently biodegradable; therefore, provided that they do not induce toxicity to the human body, microorganisms arise as an excellent component for biodegradable devices. Undoubtedly, microswimmers which incorporate motile bacteria are the most widely studied. Bacteria can be a useful component for biomedical microswimmers due to their biological robustness, inherent biodegradability, active flagellar propulsion and environmental sensing capabilities, which allow for steering under different stimuli, such as chemical gradients, temperature, light or even magnetic fields. Owing to their high speed, energy conversion efficiency and self-adaptability, bacteria-propelled microswimmers have become a powerful alternative to purely synthetic microswimmers. In addition to their motion capabilities, many bacterial strains have inherent therapeutic properties that can be exploited for combined therapies; selective tumor targeting, antitumor properties, gene delivery and detoxification capabilities are only some examples.^[140-142]

The first bacteria-based biohybrid micromachine consisted of a bacteria coupled to PS NPs or MPs. Akin et al. conjugated *Listeria monocytogenes* with gene-loaded PS NPs and observed that the biohybrid microswimmers showed enhanced cell penetration and intracellular gene expression, both in vitro and in vivo.^[143] Following the same concept, Sitti and coworkers developed biohybrid micromotors by attaching *Serratia marcescens* bacteria to PS MPs. They proved the effective propulsion of these biohybrid devices,^[144] and showed that the swimmers were chemotactic.^[145, 146] The bacterial chemotactic behavior was also exploited by other groups. For example, Park et al. conjugated *Salmonella typhimurium* bacteria to PS MPs and demonstrated their steered motion toward tumoral chemoattractants, and their effectiveness for in vivo tumor targeting (Figure 9A–C).^[147] To improve the motion performance of the small-scale swimmers and endow them with additional properties, different strategies for attaching *Escherichia coli* onto specific areas of the NPs and MPs have been developed (Figure 9D,E).^[148, 149] Luo et al. conjugated anaerobic bacteria to upconversion nanorods and Au nanorods, and proved their specific in vivo targeting toward hypoxic tumors, as well as their effective diagnostic and therapeutic properties.^[150]

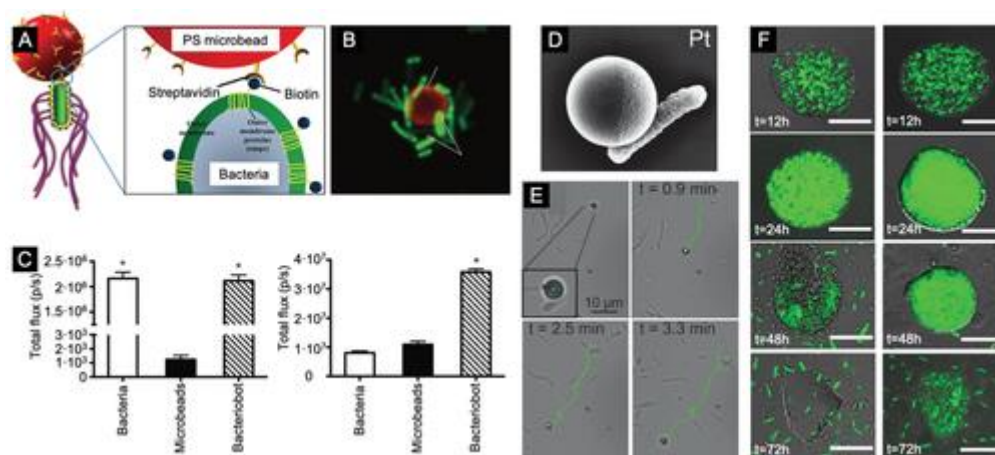


Figure 9

A) Schematic representation of the development of bacteria microswimmers using biotin-streptavidin conjugation. B) *S. typhimurium*-attached PS microbeads observed by confocal laser microscopy. C) Tumor targeting of microswimmers in a mouse model. Ex vivo bioluminescence (left) and NIR imaging (right) of the dissected tumors after treatment with bacteria, PS microbeads and bacteria-PS microswimmers. A–C) Adapted with permission under the terms of the CC-BY-NC-ND license.^[147] Copyright 2013, The Authors, published by Springer Nature. D) SEM images of *E. coli* attached to PS-Pt Janus MPs, showing preferential adhesion on the Pt cap. E) Tracking of a microswimmer with PS-Pt Janus MP and *E. coli*. D,E) Reproduced with permission.^[149] Copyright 2015, Wiley-VCH. F) Confocal microscopy images of bacteria-encapsulated alginate microbeads without (left) and with chitosan layer (right) at different times, showing the influence of chitosan layer on degradation time and subsequent bacteria release. Scale bar: 10 μ m. Adapted with permission.^[152] Copyright 2014, Wiley Periodicals, Inc.

With the aim of developing more biocompatible and biodegradable systems, other synthetic materials were integrated into bacteria-based biohybrid micromachines. The first fully biocompatible case was reported by Sukho Park and coworkers, who selectively attached *S. typhimurium* bacteria onto PEG microbeads and demonstrated their effective propulsion.^[151] Subsequently, the same group progressed to more biodegradable approaches by

replacing PEG with alginate microbeads. They observed that the motion speed, structural stability and degradation time of the microswimmers could be modified by a chitosan coating (Figure 9F).^[152] Moreover, when loading the alginate microbeads with iron oxide NPs, their motion could be controlled either by a magnetic field, for large-scale motion, or by a chemoattractant gradient, for more precise short-scale motion.^[153]

Liposomes and microemulsions can also be used as synthetic components to couple with bacteria, due to their high biocompatibility and ability to deliver different cargos. Kojima et al. reported the first example, based on *Vibrio alginolyticus* bacteria randomly attached to microliposomes, and observed that the bacteria considerably increased the motility of liposomes.^[154] Singh et al. attached double microemulsions to *E. coli* and demonstrated their enhanced chemotactic motion, tumor targeting ability and drug delivery efficiency in vitro with respect to the bare microemulsions.^[155] In a different approach, Martel and coworkers engineered biohybrid microrobots consisting of *Magnetococcus marinus* bacteria loaded with nanoliposomes onto their surface (Figure 10A,B). These bacteria naturally contain chains of iron oxide NPs, called magnetosomes, which enable them to be steered by external magnetic fields; besides, they tend to move toward low oxygen concentrations. Due to their magneto-aerotactic characteristics, the biohybrid systems can reach considerably high speeds and penetrate hypoxic tumors in vitro^[156] and in vivo.^[27] Interestingly, they observed that the nanoliposomes increased bacterial biocompatibility. These biohybrid microrobots may be a good approach for improving the therapeutic index of nanocarriers to treat hypoxic tumors.

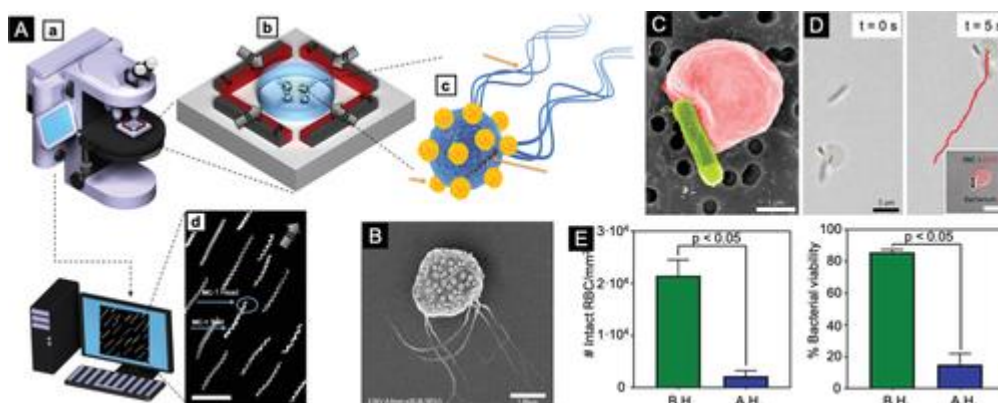


Figure 10

A) Schematic representation of the experimental setup used to track and visualize magnetotactic bacteria-liposome microrobots: a) optical microscope, b) side view of the 2D magnetic navigational setup, c) schematic of a magnetotactic bacteria-liposome microrobot and d) motility track of microrobots under the influence of the magnetic field. Images were recorded by dark field optical microscopy. Scale bar: 5 μ m. B) An SEM image of a magnetotactic bacteria-liposome microrobot. Scale bar: 10 μ m. A,B) Adapted with permission.^[156] Copyright 2014, American Chemical Society. C) An SEM image (pseudocolored red, RBC; pseudocolored green, bacterium) of an RBC microswimmer with an attached bacterium. Scale bar: 1 μ m. D) 2D propulsion trajectory of an RBC microswimmer over time. The inset displays a bacterium attached to an RBC loaded with DOX molecules. Scale bars: 5 μ m. E) NIR light-triggered hyperthermia termination switch for RBC microswimmers. Number of intact RBCs (left) and percent viable bacteria (right) before and after NIR irradiation. B.H. = before hyperthermia; A.H. = after hyperthermia. C–E) Adapted with permission.^[157] Copyright 2018, AAAS.

Alapan et al. engineered a biohybrid system based on *E. coli* attached to RBCs, which were then loaded with DOX and iron oxide NPs (Figure 10C). The microrobots were effectively self-propelled and steered by an external magnetic field (Figure 10D). They showed high flexibility and self-adaptability due to their soft cellular structure, which enabled them to traverse obstacles smaller than their actual size. The loaded DOX was released in a pH-dependent manner. Interestingly, by loading the microrobots with a NIR photothermal agent, it was possible to inactivate the bacterial activity with NIR light (Figure 10E), which could be a good strategy to prevent potential bacterial toxic effects.^[157]

In addition to bacteria, other cells or microorganisms have been tested in biohybrid microswimmers for biomedical applications. For instance, Whitesides and coworkers randomly attached PS microbeads onto the surface of *Chlamydomonas reinhardtii* flagellated microalgae and proved their phototactic motion. The microswimmers moved following light intensity gradients, and could achieve a considerable speed and travelling distance.^[158] Wang and coworkers utilized sperm cells to propel different NPs in vitro. The biohybrid systems attained high speeds and were chemotactically steered toward egg cells. When loaded with DOX-NP conjugates and incubated with ovarian cancer cells, the microswimmers showed effective tumor targeting, pH-triggered drug release and anti-tumoral effects.^[159]

Table 4 provides a summary with the characteristics of the aforementioned hybrid biodegradable small-scale swimmers based on microorganisms.

Table 4. Hybrid biodegradable small-scale swimmers based on microorganisms (biodegradable components marked in **bold**)

Motile components	Additional components	Shape (Size) ^{a/}	Functionality (additional functional part)	Degradability assay	Ref.
Bacteria	PS MPs	Spherical (2–20 µm)	Chemotaxis	nd	[145–147]
			In vivo chemotaxis and tumor targeting	nd	[147]
			Magnetic steering (Fe-PS MPs)	nd	[149]
			–	nd	[144]

Motile components	Additional components	Shape (Size) ^{a/}	Functionality (additional functional part)	Degradability assay	Ref.
	PS NPs	Spherical (40–600 nm)	In vivo drug delivery	nd	[143]
			–	nd	[148, 149]
	Upconversion nanorods	nanorods/Au Rod-like (10–20 nm × 40–60 nm)	In vivo NIR imaging (Upconversion nanorods)/photothermal therapy (Au nanorods)	nd	[150]
	PEG MPs	Spherical (10 µm)	–	nd	[151]
	Alginate MPs	Spherical (10–20 µm)	Magnetic steering (iron oxide NPs), chemotaxis	nd	[153]
			–	nd	[152]
	Microliposomes/microemulsions	Spherical (5–15 µm)	Drug delivery	nd	[155]
			–	nd	[154]
	Nanoliposomes	Spherical (200 nm)	Magnetic steering (magnetosomes), drug delivery	nd	[156]
			In vivo magnetic steering (magnetosomes), drug delivery	nd	[27]
	RBCs	RBC (5 µm)	Magnetic steering (iron oxide NPs), pH-triggered drug delivery,	nd	[157]

Motile components	Additional components	Shape (Size) ^{a/}	Functionality (additional functional part)	Degradability assay	Ref.
			light-triggered inactivation (NIR absorbing dye)		
Microalgae	PS MPs	Spherical (5 µm)	Phototaxis	nd	[158]
Sperm cells	Cd-Se NPs, iron oxide NPs, or Pt NPs	Spherical (5–10 nm)	Chemotaxis, pH-triggered drug release, chemotherapy (DOX)	nd	[159]

- ^{a/} This refers only to the shape and size of the additional components. The bacteria of the reported studies have elongated or quasispherical shape and size of 300–500 nm × 2–5 µm. Microalgae have a head of 10 µm diameter and flagella of 12 µm length. Sperm cells have a head of 1 µm and a tail of 50 µm length.

6 Conclusions and Outlook

In this review, we have assessed recent investigations on fully and partially biodegradable, motile, small-scale swimmers. The rational development of fully biodegradable small-scale-swimmer designs will be a major leap towards clinical applications. Post-application degradation of small-scale swimmers into nontoxic subproducts can greatly reduce the potential inflammation and other complications that are otherwise triggered by the nondegradable swimmer versions, eliminating the potential complexity of post-application retrieval. The application of biodegradable motile machines for therapeutic drug/cell delivery will ultimately enable the realisation of more inexpensive, safer, time and effort-saving interventional procedures in comparison to conventional approaches.

In general, small-scale swimmers roughly consist of three modules: the motion engine, the chassis and the functional building block. The latter refers to the component that targets a specific application. Note that some multifunctional materials could serve two or more purposes. Taking the biodegradation aspect into account, the motion engine is the most critical component as its choice may be highly constrained depending on the powering approach. For example, for magnetically driven micro- and nanoswimmers, the availability of magnetic materials is limited; only iron, iron-based oxides and few iron alloys exhibit both biocompatibility and biodegradability characteristics. In contrast, for those swimmers actuated by ultrasound, there is a wealth of available materials, as the actuation of these devices relies on the distinct acoustic impedance between different parts of

the swimmer. For chemically driven motors, the selection of inorganic materials (e.g., Mg, Zn) that can generate chemical propulsion in bodily fluids is also highly constrained. The use of enzymes for chemical propulsion is a promising strategy currently under investigation. Capitalizing on live microorganisms as motile components is certainly an original approach, though the safety of these microorganisms has to be carefully examined.

As for the chassis of the swimmer, there is an ample choice of materials. Note that we are currently experiencing a clear paradigm shift from rigid and solid to soft and smart small-scale swimmers.^[160-163] Therefore, a current trend in the field is the fabrication of motile micro- and nanodevices with soft building blocks and, if applicable, stimuli-responsive features. The library of biodegradable materials, such as hydrogels, conductive polymers and other supramolecular ensembles developed, is extensive and expanding. The main challenge is the machining and shaping of these materials at micro- and nanoscales in order to meet the design requirements of the swimmer (e.g., shape, stiffness). One approach consists of modifying these materials with reactive chemical moieties, which enable them to be directly processed by modern micro-additive manufacturing techniques such as TPP.^[56, 57, 70] Another approach consists of employing molding processes.^[164]

There is also plenty of scope for exploring the functional building blocks. Depending on the target application, the functional components can be drugs, therapeutic cells, photosensitive materials for photodynamic therapy or photothermal therapy,^[58, 165] hyperthermic agents^[52, 79] and sonosensitive agents for sonodynamic therapy,^[165, 166] to name just a few. While several of these agents, such as small molecule drugs and protein drugs, can be metabolized in relatively short times, others, such as inorganic NPs, will probably remain longer in the body. Furthermore, the bioresorbability of NPs is strongly influenced by their size and composition, and, in most cases, is still unclear. In general, NPs smaller than 10 nm can be resorbed through renal clearance within a few days. NPs larger than 100 nm tend to accumulate in the spleen and the liver, where they are slowly processed over weeks or even months.^[11] Note that the accumulation of NPs in the body for longer periods is not necessarily a negative aspect provided that it does not imply a risk for the patient. On the contrary, under certain circumstances, a longer stay of NPs at a specific tissue is desirable. For example, iron oxide NPs accrued in the liver have been employed for long-term tracking of disease progression with MRI.^[167] One can also envision that a directed accumulation of functional NPs at difficult-to-reach tissues using micro- and nanoswimmers could also open avenues into regenerative medicine. However, in general, the biosafety of most nanomaterials remains elusive and unaddressed.

The development of fully biodegradable small-scale swimmers is a continuing process. In addition, there is not a one-for-all swimmer configuration for all targeted therapeutic delivery scenarios, because the requirements of treating different diseases and environments at different pathological sites are diverse and specific. Although considerable success has been achieved in studies with small-scale swimmers performed in vitro, and a few remarkable examples have been demonstrated in vivo,

developing biodegradable motile devices for clinical application still has a long way to go. Besides the development of fully biodegradable swimmers, there are other main challenges to be addressed to facilitate the translation of swimmers' technologies into the clinic. New imaging technologies must be designed for the precise tracking of nano- and microdevices in vivo.^[168] Moreover, the specific control of individual swimmers and/or a "swarm" of them is fundamental to perform complex tasks and enhance their potential therapeutic effect via collective behavior.^[169]

Many aspects need to be considered for the design of a biodegradable small-scale swimmer from the viewpoint of materials, including the environment of applicable scenarios (the type of diseases, the position of pathological sites, pH, fluid speed, fluid viscosity, etc.), the interaction of the materials with the internal physiological environment of the human body, the metabolism of the materials in the body, the impact of the degraded products on human health, different degradation triggering methods (with external power, e.g. heat and light; and with internal physiological changes, e.g. local pH and enzyme concentration), and so on. A strategic method would be to design the swimmers and select the appropriate materials according to the application scenario.

We realize that the research in this topic is still in its infancy and it is not possible to determine a systematic context. However, we hope this review can provide a good source of reference and inspiration for the scientists working in this field, as more and more researchers have realised the importance of this problem while pursuing in vivo preclinical studies.

Acknowledgements

J.L.-W. and A.R.-D. contributed equally to this work. S.P. acknowledges funding from a Consolidator Grant from the European Research Council (ERC) under the European Union's Horizon 2020 Research and Innovation Programme (Grant Agreement No. 771565). X.C. is partially supported by SNF (No. CRSK-2_190451). J.L.L. and A.R. acknowledge their Ph.D. grants in the framework of the project BeMAGIC funded by the European Union's Horizon 2020 Research and Innovation Programme under the Marie Skłodowska-Curie grant agreement No. 861145. E.P. acknowledges 2017-SGR-292 project from Generalitat de Catalunya and the Spanish Ministerio de Economía, Industria y Competitividad (MAT2017-86357-C3-1-R and associated FEDER). J.P. acknowledges support from the European Research Council Starting Grant microCrysFact (ERC-2015-STG No. 677020).

Conflict of Interest

The authors declare no conflict of interest.

References

- 1B. J. Nelson, I. K. Kaliakatsos, J. J. Abbott, *Annu. Rev. Biomed. Eng.* 2010, 12, 55.
CrossrefCASPubMedWeb of Science®Google Scholar
- 2J. Li, B. E.-F. de Ávila, W. Gao, L. Zhang, J. Wang, *Sci. Robot.* 2017, 2.
CrossrefWeb of Science®Google Scholar
- 3X.-Z. Chen, M. Hoop, F. Mushtaq, E. Siringil, C. Hu, B. J. Nelson, S. Pané, *Appl. Mater. Today* 2017, 9, 37.
CrossrefPubMedWeb of Science®Google Scholar
- 4X.-Z. Chen, B. Jang, D. Ahmed, C. Hu, C. D. Marco, M. Hoop, F. Mushtaq, B. J. Nelson, S. Pané, *Adv. Mater.* 2018, 30, 1705061.
Wiley Online LibraryWeb of Science®Google Scholar
- 5J. Katuri, X. Ma, M. M. Stanton, S. Sánchez, *Acc. Chem. Res.* 2017, 50, 2.
CrossrefCASPubMedWeb of Science®Google Scholar
- 6S. Palagi, P. Fischer, *Nat. Rev. Mater.* 2018, 3, 113.
CrossrefCASWeb of Science®Google Scholar
- 7W. Z. Teo, M. Pumera, *Chem. - Eur. J.* 2016, 22, 14796.
Wiley Online LibraryCASPubMedWeb of Science®Google Scholar
- 8F. Novotný, H. Wang, M. Pumera, *Chem* 2020, 6, 867.
CrossrefCASWeb of Science®Google Scholar
- 9D. Peer, J. M. Karp, S. Hong, O. C. Farokhzad, R. Margalit, R. Langer, *Nat. Nanotechnol.* 2007, 2, 751.
CrossrefCASPubMedWeb of Science®Google Scholar
- 10M. J. Mitchell, M. M. Billingsley, R. M. Haley, M. E. Wechsler, N. A. Peppas, R. Langer, *Nat. Rev. Drug Discovery* 2021, 20, 101.
CrossrefCASPubMedWeb of Science®Google Scholar
- 11S. Wilhelm, A. J. Tavares, Q. Dai, S. Ohta, J. Audet, H. F. Dvorak, W. C. W. Chan, *Nat. Rev. Mater.* 2016, 1, 16014.
CrossrefCASWeb of Science®Google Scholar
- 12P. Fischer, A. Ghosh, *Nanoscale* 2011, 3, 557.

CrossrefCASPubMedWeb of Science®Google Scholar

- 13M. Sitti, H. Ceylan, W. Hu, J. Giltinan, M. Turan, S. Yim, E. Diller, *Proc. IEEE* 2015, 103, 205.
-

CrossrefCASPubMedWeb of Science®Google Scholar

- 14S. Wang, X. Liu, Y. Wang, D. Xu, C. Liang, J. Guo, X. Ma, *Nanoscale* 2019, 11, 14099.
-

CrossrefCASPubMedWeb of Science®Google Scholar

- 15D. Xu, Y. Wang, C. Liang, Y. You, S. Sanchez, X. Ma, *Small* 2020, 16, 1902464.
-

Wiley Online LibraryCASWeb of Science®Google Scholar

- 16J. Parmar, D. Vilela, K. Villa, J. Wang, S. Sánchez, *J. Am. Chem. Soc.* 2018, 140, 9317.
-

CrossrefCASPubMedWeb of Science®Google Scholar

- 17B. Kherzi, M. Pumera, *Nanoscale* 2016, 8, 17415.
-

CrossrefCASPubMedWeb of Science®Google Scholar

- 18T. Patiño, X. Arqué, R. Mestre, L. Palacios, S. Sánchez, *Acc. Chem. Res.* 2018, 51, 2662.
-

CrossrefCASPubMedWeb of Science®Google Scholar

- 19H. Ceylan, J. Giltinan, K. Kozielski, M. Sitti, *Lab Chip* 2017, 17, 1705.
-

CrossrefCASPubMedWeb of Science®Google Scholar

- 20J. Feng, S. Cho, *Micromachines* 2014, 5, 97.
-

CrossrefWeb of Science®Google Scholar

- 21J. J. Abbott, K. E. Peyer, M. C. Lagomarsino, L. Zhang, L. Dong, I. K. Kaliakatsos, B. J. Nelson, *Int. J. Rob. Res.* 2009, 28, 1434.
-

CrossrefWeb of Science®Google Scholar

- 22K. E. Peyer, L. Zhang, B. J. Nelson, *Nanoscale* 2013, 5, 1259.
-

CrossrefCASPubMedWeb of Science®Google Scholar

- 23A. Servant, F. Qiu, M. Mazza, K. Kostarelos, B. J. Nelson, *Adv. Mater.* 2015, 27, 2981.
-

Wiley Online LibraryCASPubMedWeb of Science®Google Scholar

-
- 24W. Gao, R. Dong, S. Thamphiwatana, J. Li, W. Gao, L. Zhang, J. Wang, *ACS Nano* 2015, 9, 117.
-

CrossrefCASPubMedWeb of Science®Google Scholar

- 25B. E.-F. de Ávila, P. Angsantikul, J. Li, W. Gao, L. Zhang, J. Wang, *Adv. Funct. Mater.* 2018, 28, 1705640.
-

Wiley Online LibraryWeb of Science®Google Scholar

- 26X. Yan, Q. Zhou, M. Vincent, Y. Deng, J. Yu, J. Xu, T. Xu, T. Tang, L. Bian, Y.-X. J. Wang, K. Kostarelos, L. Zhang, *Sci. Rob.* 2017, 2, eaaq1155.
-

CrossrefPubMedWeb of Science®Google Scholar

- 27O. Felfoul, M. Mohammadi, S. Taherkhani, D. de Lanauze, Y. Z. Xu, D. Loghin, S. Essa, S. Jancik, D. Houle, M. Lafleur, L. Gaboury, M. Tabrizian, N. Kaou, M. Atkin, T. Vuong, G. Batist, N. Beauchemin, D. Radzioch, S. Martel, *Nat. Nanotechnol.* 2016, 11, 941.
-

CrossrefCASPubMedWeb of Science®Google Scholar

- 28V. Iacovacci, L. Ricotti, E. Sinibaldi, G. Signore, F. Vistoli, A. Mencias, *Adv. Sci.* 2018, 5, 1800807.
-

Wiley Online LibraryGoogle Scholar

- 29A. A. L. Mattina, S. Mariani, G. Barillaro, *Adv. Sci.* 2020, 7, 1902872.
-

Wiley Online LibraryGoogle Scholar

- 30G. D. Cha, D. Kang, J. Lee, D.-H. Kim, *Adv. Healthcare Mater.* 2019, 8, 1801660.
-

Wiley Online LibraryPubMedWeb of Science®Google Scholar

- 31M. Vert, Y. Doi, K.-H. Hellwich, M. Hess, P. Hodge, P. Kubisa, M. Rinaudo, F. Schué, *Pure Appl. Chem.* 2012, 84, 377.
-

CrossrefCASWeb of Science®Google Scholar

- 32Y. Liu, Y. Zheng, B. Hayes, *Sci. China Mater.* 2017, 60, 377.
-

CrossrefCASWeb of Science®Google Scholar

- 33A. Terzopoulou, J. D. Nicholas, X.-Z. Chen, B. J. Nelson, S. Pané, J. Puigmartí-Luis, *Chem. Rev.* 2020, 120, 11175.
-

CrossrefCASPubMedWeb of Science®Google Scholar

- 34G. Chatzipirpiridis, C. de Marco, E. Pellicer, O. Ergeneman, J. Sort, B. J. Nelson, S. Pané, *Adv. Eng. Mater.* 2018, 20, 1800179.

Wiley Online LibraryWeb of Science®Google Scholar

- 35J. H. Young, M.-T. Wang, I. A. Brezovich, *Electron. Lett.* 1980, 16, 358.

CrossrefWeb of Science®Google Scholar

- 36M. Valko, H. Morris, M. Cronin, *Curr. Med. Chem.* 2005, 12, 1161.

CrossrefCASPubMedWeb of Science®Google Scholar

- 37E. Denkhau, K. Salnikow, *Crit. Rev. Oncol. Hematol.* 2002, 42, 35.

CrossrefCASPubMedWeb of Science®Google Scholar

- 38M. De Boeck, M. Kirsch-Volders, D. Lison, *Mutat. Res., Mol. Mech. Mutagen.* 2003, 533, 135.

CrossrefCASPubMedWeb of Science®Google Scholar

- 39G. Papanikolaou, K. Pantopoulos, *Toxicol. Appl. Pharmacol.* 2005, 202, 199.

CrossrefCASPubMedWeb of Science®Google Scholar

- 40A. Tomitaka, A. Hirukawa, T. Yamada, S. Morishita, Y. Takemura, *J. Magn. Magn. Mater.* 2009, 321, 1482.

CrossrefCASWeb of Science®Google Scholar

- 41C. C. J. Alcantara, S. Kim, S. Lee, B. Jang, P. Thakolkaran, J. Kim, H. Choi, B. J. Nelson, S. Pané, *Small* 2019, 15, 1805006.

Wiley Online LibraryPubMedWeb of Science®Google Scholar

- 42S. Laurent, D. Forge, M. Port, A. Roch, C. Robic, L. Vander Elst, R. N. Muller, *Chem. Rev.* 2008, 108, 2064.

CrossrefCASPubMedWeb of Science®Google Scholar

- 43J. Yu, B. Wang, X. Du, Q. Wang, L. Zhang, *Nat. Commun.* 2018, 9, 3260.

CrossrefPubMedWeb of Science®Google Scholar

- 44W. Chen, M. Sun, X. Fan, H. Xie, *Appl. Mater. Today* 2020, 19, 100583.

CrossrefWeb of Science®Google Scholar

- 45R. Asmatulu, M. A. Zalich, R. O. Claus, J. S. Riffle, *J. Magn. Magn. Mater.* 2005, 292, 108.

CrossrefCASWeb of Science®Google Scholar

- 46P. Pouponneau, J.-C. Leroux, S. Martel, *Biomaterials* 2009, 30, 6327.

CrossrefCASPubMedWeb of Science®Google Scholar

- 47P. Pouponneau, J.-C. Leroux, G. Soulez, L. Gaboury, S. Martel, *Biomaterials* 2011, 32, 3481.
-

CrossrefCASPubMedWeb of Science®Google Scholar

- 48J. Kim, S. Jeon, J. Lee, S. Lee, J. Lee, B. O. Jeon, J. E. Jang, H. Choi, *Sens. Actuators, B* 2018, 266, 276.
-

CrossrefCASWeb of Science®Google Scholar

- 49Y. Qiu, K. Park, *Adv. Drug Delivery Rev.* 2001, 53, 321.
-

CrossrefCASPubMedWeb of Science®Google Scholar

- 50X.-H. Qin, A. Ovsianikov, J. Stampfl, R. Liska, *BioNanomaterials* 2014, 15.
-

CrossrefGoogle Scholar

- 51C. Peters, M. Hoop, S. Pané, B. J. Nelson, C. Hierold, *Adv. Mater.* 2016, 28, 533.
-

Wiley Online LibraryCASPubMedWeb of Science®Google Scholar

- 52J. Park, C. Jin, S. Lee, J. Kim, H. Choi, *Adv. Healthcare Mater.* 2019, 8, 1900213.
-

Wiley Online LibraryWeb of Science®Google Scholar

- 53R. A. McBath, D. A. Shipp, *Polym. Chem.* 2010, 1, 860.
-

CrossrefCASWeb of Science®Google Scholar

- 54K. Knop, R. Hoogenboom, D. Fischer, U. S. Schubert, *Angew. Chem., Int. Ed.* 2010, 49, 6288.
-

Wiley Online LibraryCASPubMedWeb of Science®Google Scholar

- 55Y. Lu, D. Wang, T. Li, X. Zhao, Y. Cao, H. Yang, Y. Y. Duan, *Biomaterials* 2009, 30, 4143.
-

CrossrefCASPubMedWeb of Science®Google Scholar

- 56H. Ceylan, I. C. Yasa, O. Yasa, A. F. Tabak, J. Giltinan, M. Sitti, *ACS Nano* 2019, 13, 3353.
-

CrossrefCASPubMedWeb of Science®Google Scholar

- 57X. Wang, X.-H. Qin, C. Hu, A. Terzopoulou, X.-Z. Chen, T.-Y. Huang, K. Maniura-Weber, S. Pané, B. J. Nelson, *Adv. Funct. Mater.* 2018, 28, 1804107.
-

Wiley Online LibraryWeb of Science®Google Scholar

-
- 58M. Dong, X. Wang, X.-Z. Chen, F. Mushtaq, S. Deng, C. Zhu, H. Torlakcik, A. Terzopoulou, X.-H. Qin, X. Xiao, J. Puigmartí-Luis, H. Choi, A. P. Pêgo, Q.-D. Shen, B. J. Nelson, S. Pané, *Adv. Funct. Mater.* 2020, 30, 1910323.
-

Wiley Online LibraryCASWeb of Science®Google Scholar

- 59D. Loessner, C. Meinert, E. Kaemmerer, L. C. Martine, K. Yue, P. A. Levett, T. J. Klein, F. P. W. Melchels, A. Khademhosseini, D. W. Hutmacher, *Nat. Protoc.* 2016, 11, 727.
-

CrossrefCASPubMedWeb of Science®Google Scholar

- 60K. Thrailkill, G. Cockrell, P. Simpson, C. Moreau, J. Fowlkes, R. C. Bunn, *Clin. Chem. Lab. Med.* 2006, 44, 503
-

CrossrefCASPubMedWeb of Science®Google Scholar

- 61M. Groblewska, B. Mroczko, M. Gryko, A. Pryczynicz, K. Guzińska-Ustymowicz, B. Kędra, A. Kemonia, M. Szmitkowski, *Tumor Biol* 2014, 35, 3793.
-

CrossrefCASPubMedWeb of Science®Google Scholar

- 62J. Volatron, J. Kolosnjaj-Tabi, Y. Javed, Q. L. Vuong, Y. Gossuin, S. Neveu, N. Luciani, M. Hémadi, F. Carn, D. Alloyeau, F. Gazeau, *Sci. Rep.* 2017, 7, 40075.
-

CrossrefCASPubMedWeb of Science®Google Scholar

- 63L. S. Nair, C. T. Laurencin, *Prog. Polym. Sci.* 2007, 32, 762.
-

CrossrefCASWeb of Science®Google Scholar

- 64K. Y. Lee, D. J. Mooney, *Prog. Polym. Sci.* 2012, 37, 106.
-

CrossrefCASPubMedWeb of Science®Google Scholar

- 65N. Hu, L. Wang, W. Zhai, M. Sun, H. Xie, Z. Wu, Q. He, *Macromol. Chem. Phys.* 2018, 219, 1700540.
-

Wiley Online LibraryWeb of Science®Google Scholar

- 66S. Rutkowski, T. Si, M. Gai, M. Sun, J. Frueh, Q. He, *J. Colloid Interface Sci.* 2019, 541, 407.
-

CrossrefCASPubMedWeb of Science®Google Scholar

- 67L. Mair, S. Chowdhury, G. Paredes-Juarez, M. Guix, C. Bi, B. Johnson, B. English, S. Jafari, J. Baker-McKee, J. Watson-Daniels, O. Hale, P. Stepanov, D. Sun, Z. Baker, C. Ropp, S. Raval, D. Arifin, J. Bulte, I. Weinberg, B. Evans, D. Cappelleri, *Micromachines* 2019, 10, 230.
-

CrossrefWeb of Science®Google Scholar

-
- 68B. Porstmann, K. Jung, H. Schmechta, U. Evers, M. Pergande, T. Porstmann, H.-J. Kramm, H. Krause, *Clin. Biochem.* 1989, 22, 349.
-

CrossrefCASPubMedWeb of Science®Google Scholar

- 69M. Dash, F. Chiellini, R. M. Ottenbrite, E. Chiellini, *Prog. Polym. Sci.* 2011, 36, 981.
-

CrossrefCASWeb of Science®Google Scholar

- 70U. Bozuyuk, O. Yasa, I. C. Yasa, H. Ceylan, S. Kizilel, M. Sitti, *ACS Nano* 2018, 12, 9617.
-

CrossrefCASPubMedWeb of Science®Google Scholar

- 71T. Freier, H. S. Koh, K. Kazazian, M. S. Shoichet, *Biomaterials* 2005, 26, 5872.
-

CrossrefCASPubMedWeb of Science®Google Scholar

- 72S. M. Lim, D. K. Song, S. H. Oh, D. S. Lee-Yoon, E. H. Bae, J. H. Lee, *J. Biomater. Sci., Polym. Ed.* 2008, 19, 453.
-

CrossrefCASPubMedWeb of Science®Google Scholar

- 73I. Shitanda, M. Terashima, S. Sattayasamitsathit, Y. Hoshi, M. Itagaki, *Chem. Lett.* 2014, 44, 300.
-

CrossrefWeb of Science®Google Scholar

- 74A. M. Maier, C. Weig, P. Oswald, E. Frey, P. Fischer, T. Liedl, *Nano Lett.* 2016, 16, 906.
-

CrossrefCASPubMedWeb of Science®Google Scholar

- 75J. Li, P. Angsantikul, W. Liu, B. E.-F. de Ávila, X. Chang, E. Sandraz, Y. Liang, S. Zhu, Y. Zhang, C. Chen, W. Gao, L. Zhang, J. Wang, *Adv. Mater.* 2018, 30, 1704800.
-

Wiley Online LibraryWeb of Science®Google Scholar

- 76A. Belay, Y. Ota, K. Miyakawa, H. Shimamatsu, *J. Appl. Phycol.* 1993, 5, 235.
-

CrossrefWeb of Science®Google Scholar

- 77Z. Khan, P. Bhadouria, P. Bisen, *Curr. Pharm. Biotechnol.* 2005, 6, 373.
-

CrossrefCASPubMedWeb of Science®Google Scholar

- 78X. Yan, J. Xu, Q. Zhou, D. Jin, C. I. Vong, Q. Feng, D. H. L. Ng, L. Bian, L. Zhang, *Appl. Mater. Today* 2019, 15, 242.
-

CrossrefCASWeb of Science®Google Scholar

-
- 79X. Wang, J. Cai, L. Sun, S. Zhang, D. Gong, X. Li, S. Yue, L. Feng, D. Zhang, *ACS Appl. Mater. Interfaces* 2019, 11, 4745.
-

CrossrefCASPubMedWeb of Science®Google Scholar

- 80L. Liu, B. Chen, K. Liu, J. Gao, Y. Ye, Z. Wang, N. Qin, D. A. Wilson, Y. Tu, F. Peng, *Adv. Funct. Mater.* 2020, 30, 1910108.
-

Wiley Online LibraryCASWeb of Science®Google Scholar

- 81Y. Zhang, L. Zhang, L. Yang, C. I. Vong, K. F. Chan, W. K. K. Wu, T. N. Y. Kwong, N. W. S. Lo, M. Ip, S. H. Wong, J. J. Y. Sung, P. W. Y. Chiu, L. Zhang, *Sci. Adv.* 2019, 5, eaau9650.
-

CrossrefPubMedWeb of Science®Google Scholar

- 82K. J. Rao, F. Li, L. Meng, H. Zheng, F. Cai, W. Wang, *Small* 2015, 11, 2836.
-

Wiley Online LibraryCASPubMedWeb of Science®Google Scholar

- 83T. Xu, L.-P. Xu, X. Zhang, *Appl. Mater. Today* 2017, 9, 493.
-

CrossrefWeb of Science®Google Scholar

- 84J. Zhou, N. S. Xu, Z. L. Wang, *Adv. Mater.* 2006, 18, 2432.
-

Wiley Online LibraryCASWeb of Science®Google Scholar

- 85R. Dong, C. Wang, Q. Wang, A. Pei, X. She, Y. Zhang, Y. Cai, *Nanoscale* 2017, 9, 15027.
-

CrossrefCASPubMedWeb of Science®Google Scholar

- 86S. Du, H. Wang, C. Zhou, W. Wang, Z. Zhang, *J. Am. Chem. Soc.* 2020, 142, 2213.
-

CrossrefCASPubMedWeb of Science®Google Scholar

- 87M. Xuan, Z. Wu, J. Shao, L. Dai, T. Si, Q. He, *J. Am. Chem. Soc.* 2016, 138, 6492.
-

CrossrefCASPubMedWeb of Science®Google Scholar

- 88J. Shao, M. Abdelghani, G. Shen, S. Cao, D. S. Williams, J. C. M. van Hest, *ACS Nano* 2018, 12, 4877.
-

CrossrefCASPubMedWeb of Science®Google Scholar

- 89W. Wang, L. A. Castro, M. Hoyos, T. E. Mallouk, *ACS Nano* 2012, 6, 6122.
-

CrossrefCASPubMedWeb of Science®Google Scholar

- 90V. Garcia-Gradilla, J. Orozco, S. Sattayasamitsathit, F. Soto, F. Kuralay, A. Pourazary, A. Katzenberg, W. Gao, Y. Shen, J. Wang, *ACS Nano* 2013, 7, 9232.

CrossrefCASPubMedWeb of Science®Google Scholar

- 91Z. Wu, T. Li, W. Gao, T. Xu, B. Jurado-Sánchez, J. Li, W. Gao, Q. He, L. Zhang, J. Wang, *Adv. Funct. Mater.* 2015, 25, 3881.
-

Wiley Online LibraryCASWeb of Science®Google Scholar

- 92B. Esteban-Fernández de Ávila, P. Angsantikul, D. E. Ramírez-Herrera, F. Soto, H. Teymourian, D. Dehaini, Y. Chen, L. Zhang, J. Wang, *Sci. Robot.* 2018, 3, eaat0485.
-

CrossrefPubMedWeb of Science®Google Scholar

- 93Z. Wu, B. E.-F. de Ávila, A. Martín, C. Christianson, W. Gao, S. K. Thamphiwatana, A. Escarpa, Q. He, L. Zhang, J. Wang, *Nanoscale* 2015, 7, 13680.
-

CrossrefCASPubMedWeb of Science®Google Scholar

- 94W. Wang, W. Duan, S. Ahmed, T. E. Mallouk, A. Sen, *Nano Today* 2013, 8, 531.
-

CrossrefCASPubMedWeb of Science®Google Scholar

- 95S. Sánchez, L. Soler, J. Katuri, *Angew. Chem., Int. Ed.* 2015, 54, 1414.
-

Wiley Online LibraryCASPubMedWeb of Science®Google Scholar

- 96R. Liu, A. Sen, *J. Am. Chem. Soc.* 2011, 133, 20064.
-

CrossrefCASPubMedWeb of Science®Google Scholar

- 97N.-E. L. Saris, E. Mervaala, H. Karppanen, J. A. Khawaja, A. Lewenstam, *Clin. Chim. Acta* 2000, 294, 1.
-

CrossrefCASPubMedWeb of Science®Google Scholar

- 98S. A. Chiplonkar, R. Kawade, *Nutrition* 2012, 28, 551.
-

CrossrefCASPubMedWeb of Science®Google Scholar

- 99D. Beyersmann, *Mater. Werkst.* 2002, 33, 764.
-

Wiley Online LibraryCASWeb of Science®Google Scholar

- 100T. Sanders, Y.-M. Liu, P. B. Tchounwou, *Environ. Toxicol.* 2015, 30, 1445.
-

Wiley Online LibraryCASPubMedWeb of Science®Google Scholar

- 101W. Gao, X. Feng, A. Pei, Y. Gu, J. Li, J. Wang, *Nanoscale* 2013, 5, 4696.
-

CrossrefCASPubMedWeb of Science®Google Scholar

-
- 102J. Li, P. Angsantikul, W. Liu, B. Esteban-Fernández de Ávila, S. Thamphiwatana, M. Xu, E. Sandraz, X. Wang, J. Delezuk, W. Gao, L. Zhang, J. Wang, *Angew. Chem., Int. Ed.* 2017, 56, 2156.
-

Wiley Online LibraryCASPubMedWeb of Science®Google Scholar

- 103W. Gao, A. Uygun, J. Wang, *J. Am. Chem. Soc.* 2012, 134, 897.
-

CrossrefCASPubMedWeb of Science®Google Scholar

- 104Z. Wu, J. Li, B. E.-F. de Ávila, T. Li, W. Gao, Q. He, L. Zhang, J. Wang, *Adv. Funct. Mater.* 2015, 25, 7497.
-

Wiley Online LibraryWeb of Science®Google Scholar

- 105F. Mou, C. Chen, H. Ma, Y. Yin, Q. Wu, J. Guan, *Angew. Chem., Int. Ed.* 2013, 52, 7208.
-

Wiley Online LibraryCASPubMedWeb of Science®Google Scholar

- 106F. Mou, C. Chen, Q. Zhong, Y. Yin, H. Ma, J. Guan, *ACS Appl. Mater. Interfaces* 2014, 6, 9897.
-

CrossrefCASPubMedWeb of Science®Google Scholar

- 107B. E.-F. de Ávila, P. Angsantikul, J. Li, M. Angel Lopez-Ramirez, D. E. Ramírez-Herrera, S. Thamphiwatana, C. Chen, J. Delezuk, R. Samakapiruk, V. Ramez, M. Obonyo, L. Zhang, J. Wang, *Nat. Commun.* 2017, 8, 272.
-

CrossrefPubMedWeb of Science®Google Scholar

- 108E. Karshalev, B. Esteban-Fernández de Ávila, M. Beltrán-Gastélum, P. Angsantikul, S. Tang, R. Mundaca-Urbe, F. Zhang, J. Zhao, L. Zhang, J. Wang, *ACS Nano* 2018, 12, 8397.
-

CrossrefCASPubMedWeb of Science®Google Scholar

- 109E. Karshalev, Y. Zhang, B. Esteban-Fernández de Ávila, M. Beltrán-Gastélum, Y. Chen, R. Mundaca-Urbe, F. Zhang, B. Nguyen, Y. Tong, R. H. Fang, L. Zhang, J. Wang, *Nano Lett.* 2019, 19, 7816.
-

CrossrefCASPubMedWeb of Science®Google Scholar

- 110C. Chen, E. Karshalev, J. Li, F. Soto, R. Castillo, I. Campos, F. Mou, J. Guan, J. Wang, *ACS Nano* 2016, 10, 10389.
-

CrossrefCASPubMedWeb of Science®Google Scholar

- 111J. Li, S. Thamphiwatana, W. Liu, B. Esteban-Fernández de Ávila, P. Angsantikul, E. Sandraz, J. Wang, T. Xu, F. Soto, V. Ramez, X. Wang, W. Gao, L. Zhang, J. Wang, *ACS Nano* 2016, 10, 9536.

CrossrefCASPubMedWeb of Science®Google Scholar

- 112M. Zhou, T. Hou, J. Li, S. Yu, Z. Xu, M. Yin, J. Wang, X. Wang, *ACS Nano* 2019, 13, 1324.
-

CrossrefCASPubMedWeb of Science®Google Scholar

- 113S. Sattayasamitsathit, H. Kou, W. Gao, W. Thavarajah, K. Kaufmann, L. Zhang, J. Wang, *Small* 2014, 10, 2830.
-

Wiley Online LibraryCASPubMedWeb of Science®Google Scholar

- 114J. G. Croissant, Y. Fatieiev, N. M. Khashab, *Adv. Mater.* 2017, 29, 1604634.
-

Wiley Online LibraryCASWeb of Science®Google Scholar

- 115K. S. Finnie, D. J. Waller, F. L. Perret, A. M. Krause-Heuer, H. Q. Lin, J. V. Hanna, C. J. Barbé, *J. Sol-Gel Sci. Technol.* 2009, 49, 12.
-

CrossrefCASWeb of Science®Google Scholar

- 116M. Xuan, J. Shao, X. Lin, L. Dai, Q. He, *ChemPhysChem* 2014, 15, 2255.
-

Wiley Online LibraryCASPubMedWeb of Science®Google Scholar

- 117X. Ma, A. Jannasch, U.-R. Albrecht, K. Hahn, A. Miguel-López, E. Schäffer, S. Sánchez, *Nano Lett.* 2015, 15, 7043.
-

CrossrefCASPubMedWeb of Science®Google Scholar

- 118X. Arqué, A. Romero-Rivera, F. Feixas, T. Patiño, S. Osuna, S. Sánchez, *Nat. Commun.* 2019, 10, 2826.
-

CrossrefPubMedWeb of Science®Google Scholar

- 119T. Patiño, N. Feiner-Gracia, X. Arqué, A. Miguel-López, A. Jannasch, T. Stumpp, E. Schäffer, L. Albertazzi, S. Sánchez, *J. Am. Chem. Soc.* 2018, 140, 7896.
-

CrossrefCASPubMedWeb of Science®Google Scholar

- 120A. C. Hortelão, T. Patiño, A. Perez-Jiménez, À. Blanco, S. Sánchez, *Adv. Funct. Mater.* 2018, 28, 1705086.
-

Wiley Online LibraryWeb of Science®Google Scholar

- 121D. A. Wilson, R. J. M. Nolte, J. C. M. van Hest, *Nat. Chem.* 2012, 4, 268.
-

CrossrefCASPubMedWeb of Science®Google Scholar

- 122Y. Tu, F. Peng, A. A. M. André, Y. Men, M. Srinivas, D. A. Wilson, *ACS Nano* 2017, 11, 1957.

CrossrefCASPubMedWeb of Science®Google Scholar

- 123Y. Tu, F. Peng, P. B. White, D. A. Wilson, *Angew. Chem., Int. Ed.* 2017, 56, 7620.

Wiley Online LibraryCASPubMedWeb of Science®Google Scholar

- 124B. J. Toebes, L. K. E. A. Abdelmohsen, D. A. Wilson, *Polym. Chem.* 2018, 9, 3190.

CrossrefCASWeb of Science®Google Scholar

- 125B. J. Toebes, F. Cao, D. A. Wilson, *Nat. Commun.* 2019, 10, 5308.

CrossrefPubMedWeb of Science®Google Scholar

- 126Z. Wu, Y. Wu, W. He, X. Lin, J. Sun, Q. He, *Angew. Chem., Int. Ed.* 2013, 52, 7000.

Wiley Online LibraryCASPubMedWeb of Science®Google Scholar

- 127N. Hu, M. Sun, X. Lin, C. Gao, B. Zhang, C. Zheng, H. Xie, Q. He, *Adv. Funct. Mater.* 2018, 28, 1705684.

Wiley Online LibraryWeb of Science®Google Scholar

- 128Z. Wu, X. Lin, X. Zou, J. Sun, Q. He, *ACS Appl. Mater. Interfaces* 2015, 7, 250.

CrossrefCASPubMedWeb of Science®Google Scholar

- 129M. V. Lomova, A. I. Brichkina, M. V. Kiryukhin, E. N. Vasina, A. M. Pavlov, D. A. Gorin, G. B. Sukhorukov, M. N. Antipina, *ACS Appl. Mater. Interfaces* 2015, 7, 11732.

CrossrefCASPubMedWeb of Science®Google Scholar

- 130B. H. C. M. T. Prinsen, M. G. M. de Sain-van der Velden, *Clin. Chim. Acta* 2004, 347, 1.

CrossrefCASPubMedWeb of Science®Google Scholar

- 131N. Sugai, Y. Nakai, Y. Morita, T. Komatsu, *ACS Appl. Nano Mater* 2018, 1, 3080.

CrossrefCASWeb of Science®Google Scholar

- 132N. Sugai, Y. Morita, T. Komatsu, *Chem. - Asian J.* 2019, 14, 2953.

Wiley Online LibraryCASPubMedWeb of Science®Google Scholar

- 133Y. Nakai, N. Sugai, H. Kusano, Y. Morita, T. Komatsu, *ACS Appl. Nano Mater.* 2019, 2, 4891.

CrossrefCASWeb of Science®Google Scholar

-
- 134F.-L. Mi, Y.-C. Tan, H.-F. Liang, H.-W. Sung, *Biomaterials* 2002, 23, 181.
-

CrossrefCASPubMedWeb of Science®Google Scholar

- 135A. X. Lu, Y. Liu, H. Oh, A. Gargava, E. Kendall, Z. Nie, D. L. DeVoe, S. R. Raghavan, *ACS Appl. Mater. Interfaces* 2016, 8, 15676.
-

CrossrefCASPubMedWeb of Science®Google Scholar

- 136H. Choi, B. W. Hwang, K. M. Park, K. S. Kim, S. K. Hahn, *Part. Part. Syst. Charact.* 2020, 37, 1900418.
-

Wiley Online LibraryCASWeb of Science®Google Scholar

- 137M. Wan, H. Chen, Q. Wang, Q. Niu, P. Xu, Y. Yu, T. Zhu, C. Mao, J. Shen, *Nat. Commun.* 2019, 10, 966.
-

CrossrefPubMedWeb of Science®Google Scholar

- 138G. Zhao, T. H. Seah, M. Pumera, *Chem. - Eur. J.* 2011, 17, 12020.
-

Wiley Online LibraryCASPubMedWeb of Science®Google Scholar

- 139A. Pena-Francesch, J. Giltinan, M. Sitti, *Nat. Commun.* 2019, 10, 3188.
-

CrossrefPubMedWeb of Science®Google Scholar

- 140N. S. Forbes, *Nat. Rev. Cancer* 2010, 10, 785.
-

CrossrefCASPubMedWeb of Science®Google Scholar

- 141R. W. Carlsen, M. Sitti, *Small* 2014, 10, 3831.
-

Wiley Online LibraryCASPubMedWeb of Science®Google Scholar

- 142Z. Hosseini-doust, B. Mostaghaci, O. Yasa, B.-W. Park, A. V. Singh, M. Sitti, *Adv. Drug Delivery Rev.* 2016, 106, 27.
-

CrossrefCASPubMedWeb of Science®Google Scholar

- 143D. Akin, J. Sturgis, K. Ragheb, D. Sherman, K. Burkholder, J. P. Robinson, A. K. Bhunia, S. Mohammed, R. Bashir, *Nat. Nanotechnol.* 2007, 2, 441.
-

CrossrefCASPubMedWeb of Science®Google Scholar

- 144B. Behkam, M. Sitti, *Appl. Phys. Lett.* 2007, 90, 023902.
-

CrossrefCASWeb of Science®Google Scholar

- 145D. Kim, A. Liu, E. Diller, M. Sitti, *Biomed. Microdevices* 2012, 14, 1009.
-

CrossrefCASPubMedWeb of Science®Google Scholar

-
- 146J. Zhuang, R. W. Carlsen, M. Sitti, *Sci. Rep.* 2015, 5, 11403.
-

CrossrefPubMedWeb of Science®Google Scholar

- 147S. J. Park, S.-H. Park, S. Cho, D.-M. Kim, Y. Lee, S. Y. Ko, Y. Hong, H. E. Choy, J.-J. Min, J.-O. Park, S. Park, *Sci. Rep.* 2013, 3, 3394.
-

CrossrefPubMedWeb of Science®Google Scholar

- 148R. Fernandes, M. Zuniga, F. R. Sassine, M. Karakoy, D. H. Gracias, *Small* 2011, 7, 588.
-

Wiley Online LibraryCASPubMedWeb of Science®Google Scholar

- 149M. M. Stanton, J. Simmchen, X. Ma, A. Miguel-López, S. Sánchez, *Adv. Mater. Interfaces* 2016, 3, 1500505.
-

Wiley Online LibraryCASWeb of Science®Google Scholar

- 150C.-H. Luo, C.-T. Huang, C.-H. Su, C.-S. Yeh, *Nano Lett.* 2016, 16, 3493.
-

CrossrefCASPubMedWeb of Science®Google Scholar

- 151S. Cho, S. J. Park, S. Y. Ko, J.-O. Park, S. Park, *Biomed. Microdevices* 2012, 14, 1019.
-

CrossrefCASPubMedWeb of Science®Google Scholar

- 152S. J. Park, Y. K. Lee, S. Cho, S. Uthaman, I.-K. Park, J.-J. Min, S. Y. Ko, J.-O. Park, S. Park, *Biotechnol. Bioeng.* 2015, 112, 769.
-

Wiley Online LibraryCASPubMedWeb of Science®Google Scholar

- 153D. Li, H. Choi, S. Cho, S. Jeong, Z. Jin, C. Lee, S. Y. Ko, J.-O. Park, S. Park, *Biotechnol. Bioeng.* 2015, 112, 1623.
-

Wiley Online LibraryCASPubMedWeb of Science®Google Scholar

- 154M. Kojima, Z. Zhang, M. Nakajima, K. Ooe, T. Fukuda, *Sens. Actuators, B* 2013, 183, 395.
-

CrossrefCASWeb of Science®Google Scholar

- 155A. V. Singh, Z. Hosseinidoust, B.-W. Park, O. Yasa, M. Sitti, *ACS Nano* 2017, 11, 9759.
-

CrossrefCASPubMedWeb of Science®Google Scholar

- 156S. Taherkhani, M. Mohammadi, J. Daoud, S. Martel, M. Tabrizian, *ACS Nano* 2014, 8, 5049.

CrossrefCASPubMedWeb of Science®Google Scholar

- 157Y. Alapan, O. Yasa, O. Schauer, J. Giltinan, A. F. Tabak, V. Sourjik, M. Sitti, *Sci. Robot.* 2018, 3, eaar4423.

CrossrefPubMedWeb of Science®Google Scholar

- 158D. B. Weibel, P. Garstecki, D. Ryan, W. R. DiLuzio, M. Mayer, J. E. Seto, G. M. Whitesides, *Proc. Natl. Acad. Sci.* 2005, 102, 11963.

CrossrefCASPubMedWeb of Science®Google Scholar

- 159C. Chen, X. Chang, P. Angsantikul, J. Li, B. Esteban-Fernández de Ávila, E. Karshalev, W. Liu, F. Mou, S. He, R. Castillo, Y. Liang, J. Guan, L. Zhang, J. Wang, *Adv. Biosyst.* 2018, 2, 1700160.

Wiley Online LibraryWeb of Science®Google Scholar

- 160H.-W. Huang, M. S. Sakar, A. J. Petruska, S. Pané, B. J. Nelson, *Nat. Commun.* 2016, 7, 12263.

CrossrefCASPubMedWeb of Science®Google Scholar

- 161L. Hines, K. Petersen, G. Z. Lum, M. Sitti, *Adv. Mater.* 2017, 29, 1603483.

Wiley Online LibraryCASWeb of Science®Google Scholar

- 162L. Ricotti, B. Trimmer, A. W. Feinberg, R. Raman, K. K. Parker, R. Bashir, M. Sitti, S. Martel, P. Dario, A. Menciassi, *Sci. Robot.* 2017, 2.

CrossrefPubMedGoogle Scholar

- 163C. Hu, S. Pané, B. J. Nelson, *Annu. Rev. Control Robot. Auton. Syst.* 2018, 1, 53.

CrossrefGoogle Scholar

- 164C. de Marco, C. C. J. Alcântara, S. Kim, F. Briatico, A. Kadioglu, G. de Bernardis, X. Chen, C. Marano, B. J. Nelson, S. Pané, *Adv. Mater. Technol.* 2019, 4, 1900332.

Wiley Online LibraryWeb of Science®Google Scholar

- 165X.-Z. Chen, J.-H. Liu, M. Dong, L. Müller, G. Chatzipirpiridis, C. Hu, A. Terzopoulou, H. Torlakcik, X. Wang, F. Mushtaq, J. Puigmartí-Luis, Q.-D. Shen, B. J. Nelson, S. Pané, *Mater. Horiz.* 2019, 6, 1512.

CrossrefCASWeb of Science®Google Scholar

- 166F. Mushtaq, H. Torlakcik, M. Hoop, B. Jang, F. Carlson, T. Grunow, N. Läubli, A. Ferreira, X.-Z. Chen, B. J. Nelson, S. Pané, *Adv. Funct. Mater.* 2019, 29, 1808135.

Wiley Online LibraryWeb of Science®Google Scholar

- 167B. Pelaz, C. Alexiou, R. A. Alvarez-Puebla, F. Alves, A. M. Andrews, S. Ashraf, L. P. Balogh, L. Ballerini, A. Bestetti, C. Brendel, S. Bosi, M. Carril, W. C. W. Chan, C. Chen, X. Chen, X. Chen, Z. Cheng, D. Cui, J. Du, C. Dullin, A. Escudero, N. Feliu, M. Gao, M. George, Y. Gogotsi, A. Grünweller, Z. Gu, N. J. Halas, N. Hampp, R. K. Hartmann, M. C. Hersam, P. Hunziker, J. Jian, X. Jiang, P. Jungebluth, P. Kadhiresan, K. Kataoka, A. Khademhosseini, J. Kopeček, N. A. Kotov, H. F. Krug, D. S. Lee, C.-M. Lehr, K. W. Leong, X.-J. Liang, M. L. Lim, L. M. Liz-Marzán, X. Ma, P. Macchiarini, H. Meng, H. Möhwald, P. Mulvaney, A. E. Nel, S. Nie, P. Nordlander, T. Okano, J. Oliveira, T. H. Park, R. M. Penner, M. Prato, V. Puntès, V. M. Rotello, A. Samarakoon, R. E. Schaak, Y. Shen, S. Sjöqvist, A. G. Skirtach, M. G. Soliman, M. M. Stevens, H.-W. Sung, B. Z. Tang, R. Tietze, B. N. Udugama, J. S. VanEpps, T. Weil, P. S. Weiss, I. Willner, Y. Wu, L. Yang, Z. Yue, Q. Zhang, Q. Zhang, X.-E. Zhang, Y. Zhao, X. Zhou, W. J. Parak, *ACS Nano* 2017, 11, 2313.
-

CrossrefCASPubMedWeb of Science®Google Scholar

- 168S. Pané, J. Puigmartí-Luis, C. Bergeles, X. Chen, E. Pellicer, J. Sort, V. Počepcová, A. Ferreira, B. J. Nelson, *Adv. Mater. Technol.* 2019, 4, 1800575.
-

Wiley Online LibraryWeb of Science®Google Scholar

- 169Q. Wang, L. Zhang, *ACS Nano* 2021, 15, 149.
-

CrossrefCASPubMedWeb of Science®Google Scholar